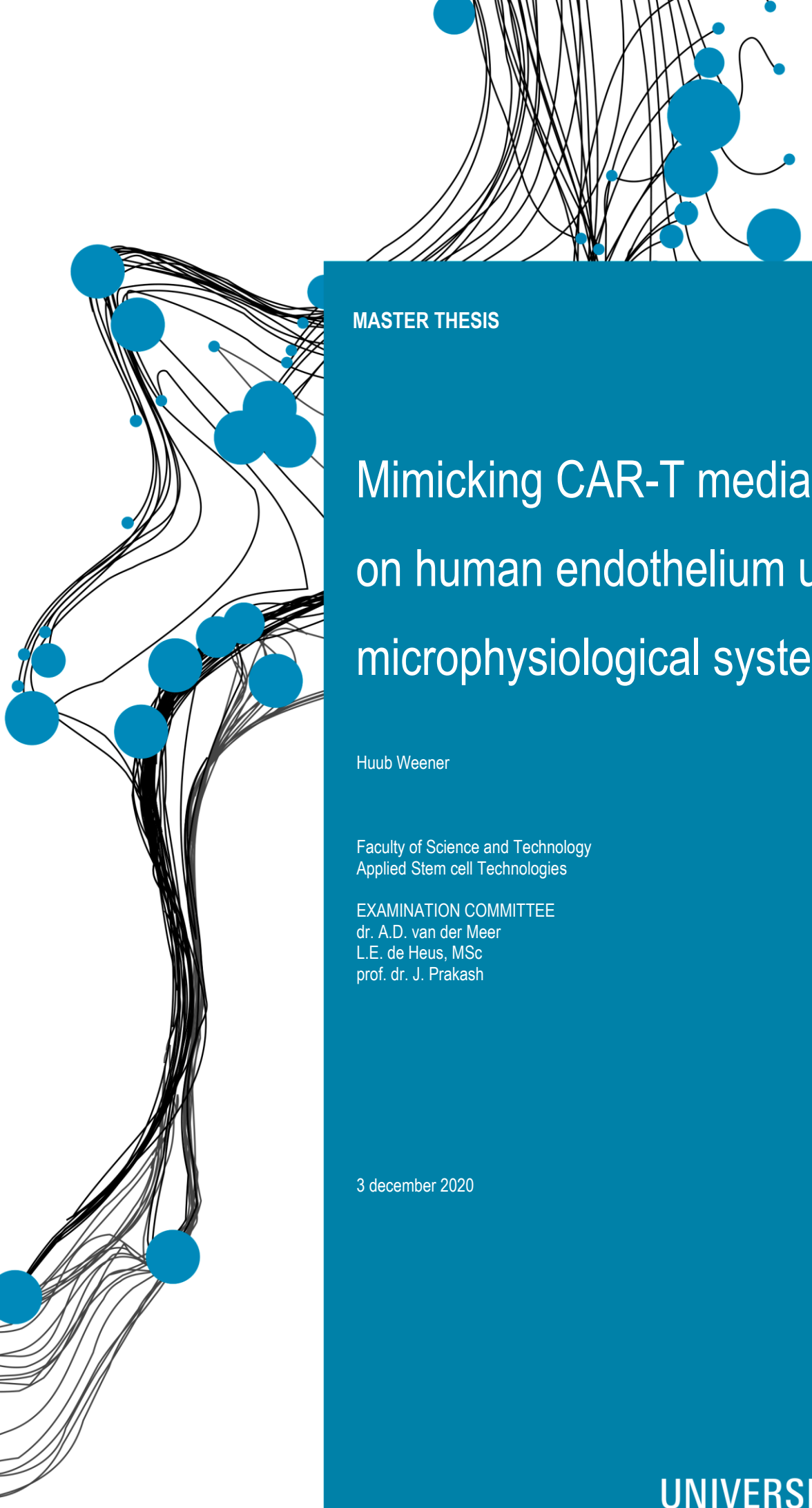

MASTER THESIS

Mimicking CAR-T mediated CRS on human endothelium using microphysiological systems

Huub Weener

Faculty of Science and Technology
Applied Stem cell Technologies

EXAMINATION COMMITTEE
dr. A.D. van der Meer
L.E. de Heus, MSc
prof. dr. J. Prakash

3 december 2020

UNIVERSITY OF TWENTE.

Abstract

Chimeric antigen receptor T cell (CAR-T cell) immunotherapy is a novel therapy that has been approved in Europe and the United States against haematological malignancies. Current therapies have CAR-T cells release significant amounts of cytokines that help in the breakdown of the tumour, but also have adverse effects known as a cytokine release syndrome. The CAR-T cells release too many cytokines, destroying surrounding tissues and hospitalizing the patients. The endothelium is broken down by these cytokines, further enhancing their release. Current disease models lack in mimicking this interaction between cytokines and endothelium, so in this study a microphysiological blood vessel-on-chip is used to mimic the interaction that takes place *in vivo*. This system is seeded with human embryonic stem cell derived endothelial cells that are cultured in a circular collagen channel. After 72 hours of culturing, the endothelial cells had formed a monolayer. Cytokines harvested from CAR-T cells co-cultured with tumour cells were then applied for 24 hours. Their effect was measured using fluorescent angiography and immunostainings for DNA, VE-cadherin, ICAM-1, and actin. The results show that there is a decrease in cell viability if the cytokine concentration in the media is increased, indicating that the effect of CAR-T cell derived cytokines on human endothelium can be mimicked in the proposed device.

Contents

Introduction

Over the last decade, there has been an increase in the use of cellular immunotherapies as a treatment for certain types of cancer [1]. One of these emerging treatments is the chimeric antigen receptor T cells (CAR-T cells) that can be derived from a patient's own T cells. Both the Food and Drug Administration (FDA) in the United states and the European Medicines Agency (EMA) have approved two treatments, Kymriah and Yescarta, for varying hematologic malignancies using anti-cluster of differentiation 19 (CD19) CAR-T cells. For anti-CD19 CAR-T cell therapies, T cells are collected from the blood of a patient, and genetically engineered to target the CD19 protein that is commonly found on B lymphocytes and their respective tumour cells. Besides these tested and proven drugs, 171 anti-CD19 CAR-T cell therapies are currently active, or recruiting in phases 1, 2, or 3 of clinical trials [2]. An overview of these clinical trials is given in Table 1. Different generations of CAR-T cell therapy exist, with varying co-stimulators and varying degrees of efficacy [3]. A schematic overview of different CAR constructs that can be engineered in T-cells is shown in Figure 1.

Table 1: Overview of clinical trials testing anti-CD19 CAR-T cell therapies, July 2020 [2]

Study phase	Total studies	Recruiting studies	Active studies, not recruiting	Enrolled patients
Phase 1	90	67	23	3087
Phase 1/ 2	61	48	13	4002
Phase 2	19	14	5	1340
Phase 2/ 3	1	1	0	10
Total	171	130	41	8439

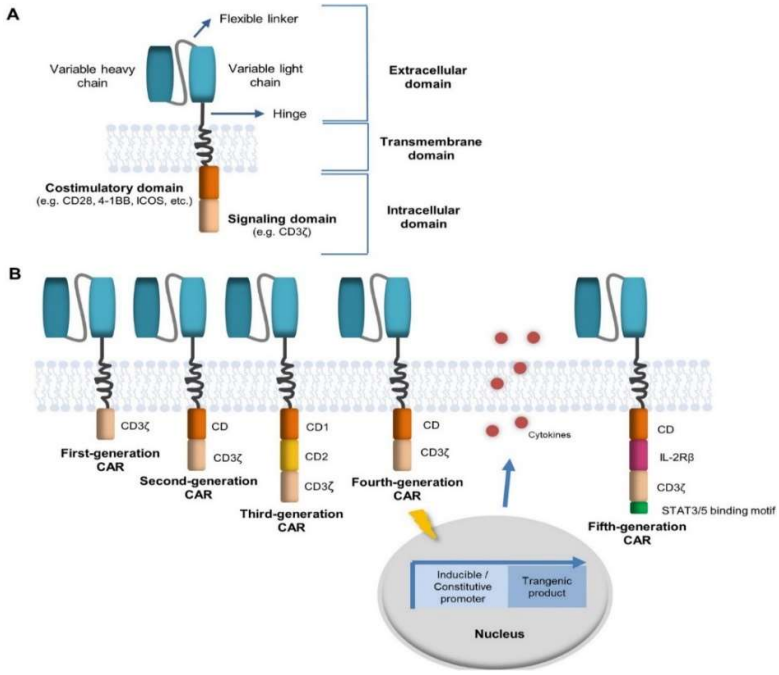

Figure 1: Overview of a CAR construct (A) and differences in CAR constructs over multiple generations (B). The extracellular domain connects with the protein of interest presented on the tumour cell, which activates the intracellular domain and therefore the T-cell. Different generations of CAR-T cells have been developed, with changes in co-stimulatory domains (generation 2, 3, 5) or inducible switches (generation 4). Figure courtesy of Abreu et al [4].

When a CAR-T cell is activated, the T cell starts to act as a normal part of the immune system. The T cells notice the CD19 rich tumour cells and secrete cytokines to kill the tumours. However, the CAR-T cell therapy consists of several millions of protein-specific T cells that are injected in the blood stream

in patient dependent doses. This can create an overshooting inflammatory response, that recruits bystander immune cells like macrophages, monocytes, and dendrites, which in turn secrete more cytokines. These cytokines help with the further recruitment of bystander immune cells. This positive feedback loop becomes unmanageable in some patients, damaging surrounding tissue [5]. This is commonly known as a cytokine release syndrome (CRS), and has different grades of severity in patients. A summary of the CAR-T reaction on a cellular level is shown in Figure 2J.

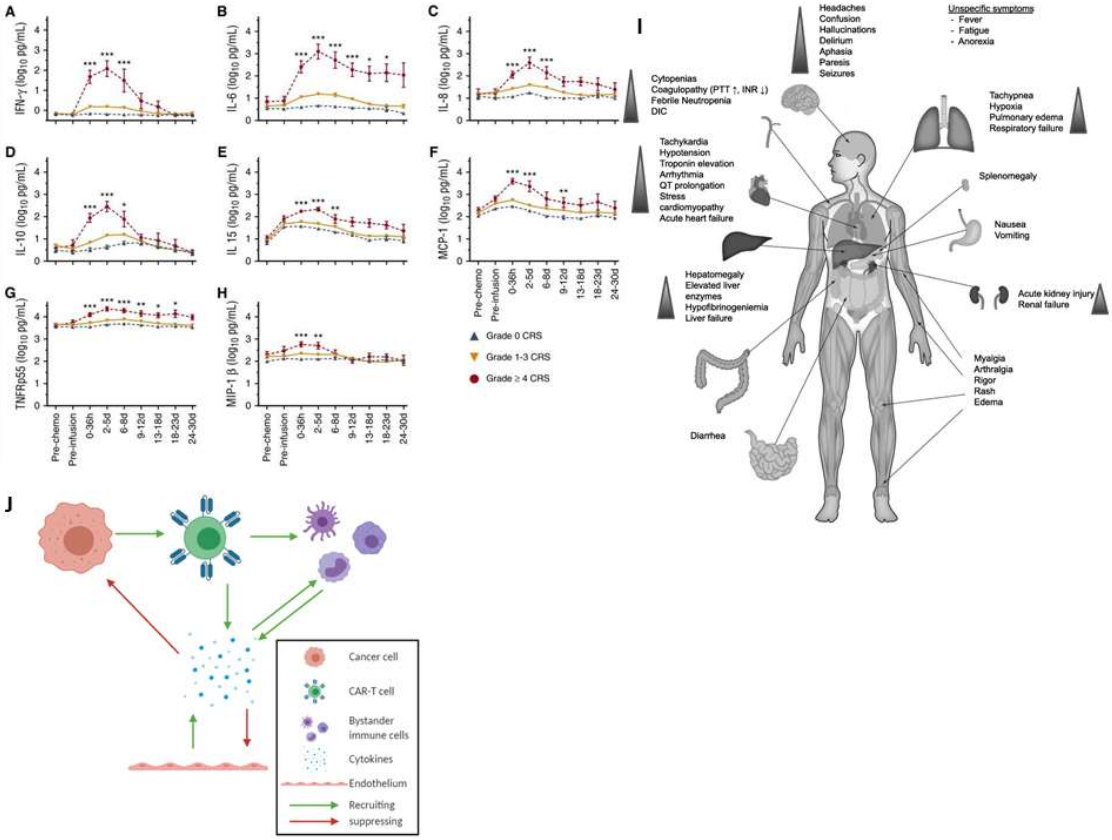

*Figure 2: Dynamics, symptoms, and pathophysiology of CAR-T mediated CRS. (A-H): Concentrations of cytokines that are related to CRS severity and its dynamics. P values are determined by Kruskal-Willis test. ***P < .0001; **P ranges from >.0001 to <.001; *P ranges from >.001 to <.005 [6]. (I): Symptoms related to CRS categorized per organ. Abbreviations: DIC: disseminated intravascular coagulation; INR: international normalized ratio; PTT: partial thromboplastin time [5]. (J): Pathophysiology of CRS on a cellular level. Graphical presentation of the pathophysiology of CRS, as described by Neelapu et al [7]. Sub-figure (J) created with BioRender.com.*

CRS is characterized by symptoms ranging between mild and life threatening [8]. A summary of these symptoms is seen in Figure 2I. Mild cases of CRS might only be affected by a higher body temperature, or a headache due to the inflammatory reaction that occurs throughout the body. In such mild cases additional treatment is not necessary, but patients should be monitored in the hospital in case symptoms do become worse. More severe cases are affected by organ toxicity, hypotension, and vascular leak [9]. These severe cases require ventilation support, administration of vasopressors, and IL-6 blockers, like tocilizumab. CRS is indicated by elevated levels of pro-inflammatory cytokines, like IL-2, IL-6 and IFN-γ, and by more common inflammatory biomarkers, like C-reactive protein and ferritin [10]. The dynamics of the concentrations of these cytokines *in vivo* is depicted in Figure 2A-H. This creates a complex interaction between pro- and anti-inflammatory cytokines that attempt to regulate one another [11].

While knowledge is being obtained about the symptoms of CRS and how treatment might be effective, it is currently unknown how certain factors in patients affect the severity. CRS severity might be linked to CAR-T dosage [12], tumour burden [13], and pre-activated endothelium [6]. CAR-T dosage and tumour burden might affect the total concentration of cytokines that is released into the blood stream. With a high dosage or burden, the peak concentration might be too high for the surrounding tissues, which results in CRS [7].

Endothelial complications in CAR-T related CRS

One of the affected tissues in CRS is the endothelium, which is the inner layer of cells in blood vessels. The endothelium normally acts as a barrier to keep the blood within its vessels. A degradation of this barrier function leads to leaking vessels, formation of blood clots, an increase of adhesion molecules (vascular cell adhesion marker 1; VCAM-1, and intracellular adhesion marker 1; ICAM-1), and macrophage recruitment into the tissue [14]. The adhesion markers create a more favourable environment for immune cells to adhere to the endothelium, where they penetrate the endothelium into the surrounding tissue. Due to CRS, both adhesion markers are upregulated in endothelial cells throughout the whole body, causing the immune cells to penetrate the endothelial barrier throughout the whole body, instead of just the tumour site [15]. A summary of the endothelial breakdown is shown in Figure 3. The endothelium degrades under high concentrations of cytokines. If the endothelium is already damaged due to a prior treatment of the malignancy [16] or another inflammation in the body, a smaller concentration of cytokines can be managed before the endothelium is further damaged.

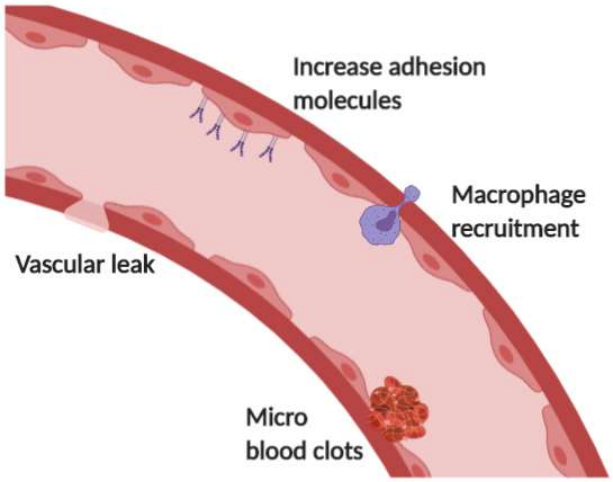

Figure 3: Endothelial dysfunction following CAR-T mediated CRS. Due to the increase in cytokines, the endothelium barrier breaks down, creating vascular leak and an increase in adhesion molecules. This leads to the formation of micro blood clots and the recruitment of macrophages. Figure created with BioRender.com.

Multiple clinical trials have been performed where damage to the endothelium was noticed as an adverse effect of the CAR-T cell therapy. A summary of these clinical trials is shown in Table 2. In these clinical trials, neurotoxicity is also mentioned since the integrity of the blood-brain barrier seems to be affected by the cytokines the same way as other capillaries in the body.

Table 2: Overview of clinical trials and case studies of CAR-T cell therapy where adverse effects on the endothelium or haemostasis were found.

Study	CAR-T cell type (cell dose/ kg)	Cohort	Cases of CRS	Remarks
Gust et al [12]	CD19-CAR-T w/ 4-1BB domain. (Doses variated)	N = 133 (NHL = 63; ALL = 47; CLL = 24)	93 (70%) 16 severe (12%)	Found microthrombi and multifocal microhaemorrhages. Consistent breakdown of the blood-brain barrier.
Bouchkouj et al [17]	CD19-CAR-T (median dose $2x10^6$)	N=108	94 (86%) 13 severe (12%)	Capillary leak as severe form of CRS.
Jiang et al [13]	CD19-CAR-T ($0.5\text{-}1x10^7$)	N=53	53 (100%) 19 severe (36%)	Coagulopathy related diseases were more common in severe CRS patients. Increase of CD31 (endothelial cell marker) in serum.
Gust et al [18]	CD19-CAR-T (dose unknown)	N=43 1-26 years old	40 (93%) 10 severe (23%)	Found correlation between neurotoxicity and CRS, but not between endothelium activation and neurotoxicity. Could be because of small control (n=2), or because of younger patients where endothelium activation is less common.
Stahl et al [19]	CD19-CAR-T ($2.58x10^8$, weight unknown)	N=1	1 (100%)	Progressive EC leakage noticed over the time of CRS.
Jia et al [20]	CD19 CAR-T ($4.9x10^6$) + CD19/22-CAR-T ($4.7x10^6$)	N=1	1 (100%)	Found capillary leak with hypoalbuminemia during CRS.
Liu et al [21]	CD19-CAR-T ($1x\ 1x10^7$) + BCMA CAR-T ($2x\ 1x10^7$)	N = 1	1 (100%)	Found venous thromboembolism in upper left leg and severe bleeding tendency.

With the symptoms found in the summary of clinical trials, it is thought that the endothelium is in an activated state, which is the result of an inflammatory reaction. As with any inflammatory reaction, the permeability of the endothelium is increased during CRS. Due to the high concentrations of cytokines, the permeability of the vessels is increased much more than normal. This creates an opportunity for more immune cells to penetrate the endothelium, increases the flux of serum into the tissue, and causes extensive vascular leak [6], [12], [22]. The degradation of the endothelium throughout the entire body by the interaction of the activated endothelium with the immune system, enhances the effect of degrading organ function which might ultimately lead to multi-organ failure [23], [24].

Some studies show changes in the haemostasis of a patient, where disseminated intravascular coagulation (DIC) is one of the symptoms [12], [13], [21], [25]. DIC occurs when multiple blood clots are formed and use up blood platelets, causing a tendency of haemorrhaging due to the lack of platelets. The platelets are also decreased since they stick to the walls of the endothelium, creating two pathways that cause thrombocytopenia [26]. Both DIC and thrombocytopenia are symptoms that are caused by the activation of endothelial cells, further acknowledging the importance of the endothelium in CRS. Therefore, it is important that this interaction between the endothelium and CAR-T mediated CRS is modelled appropriately.

Current models for endothelial dysfunction in CAR-T

Pre-clinical models can be divided in two categories: *in vitro* models and animal models. Both models are an essential step in the safety assessment of a new drug. *In vitro* models are used to model the drug on human cells, but lack the complexity of a whole organism that contains multiple cell types with a complex interaction. Animal models do provide this complexity, but do not react in the same way to a drug as a human being, and are time consuming [27].

Some animal models found CRS as an adverse effect to CAR-T treatment [28], [29]. Both studies found an increase in IL-6, which is also increased in human patients, but are contradicting in the source of IL-6, one mentioning the endothelial cells and the other macrophages. It might be the case that both are contributing to the release of IL-6. Other animal models that found signs of CRS in mice, mention that a lower concentration of cytokines is observed in animal models, due to a lower dose of injected CAR-T cells when compared to patients [30]. In a model by *Giavridis et al*, a potential treatment of CRS was explored by blocking IL-1 receptors [31].

In vitro models consist of all cellular models that are maintained in the biological lab. These models have different stages of complexity, ranging from a 2D single cell layer in a wells plate, to 3D tissues that are grown in polymer constructs or bioreactors. For *in vitro* models of endothelial reaction to CRS activating therapeutics, studies make use of either 2D cell layers in well plates [32]–[34], or 3D scaffolding [35]. For the current models, human umbilical vein endothelial cells (HUVECs) are commonly combined with peripheral blood mononuclear cells (PBMCs). Other possibilities are the use of endothelial cells derived from stem cells [36], or using diluted whole blood to obtain an immune response [37].

In vitro models of CRS have also been used to find in which cells CRS originates [38], or have contributed to new treatments of CRS [39], [40]. One model for endothelial damage caused by CD123 targeting CAR-T cells was found [41]. This model found that the released TNF-α and IFN-γ damaged the endothelial cells in a co-culture but could be reversed by adding their respective blockers.

Organ-on-chip models for endothelial dysfunction

Due to the lack of human *in vitro* models for endothelial dysfunction in CRS, and the fact that animal models might not be reacting in the same way, new models are needed that combine the advantages of both models. This is possible by using advanced microphysiological systems, which are small *in vitro* models that have more complexity by incorporating flow, multiple cell types, and 3D cell culture [42]. These systems, also known as organs-on-chips, create models that are closer to the *in vivo* situation by mimicking the mechanical and chemical properties of the human body.

There are multiple goals that can be reached by using a blood vessel-on-chip model. The model can be used to measure a barrier function of the endothelium, can simulate blood coagulation, or can be used to examine the vascularization under different circumstances. These goals could be reached in a 2D or a 3D manner. A summary of different blood vessel-on-chip systems is shown in Figure 4.

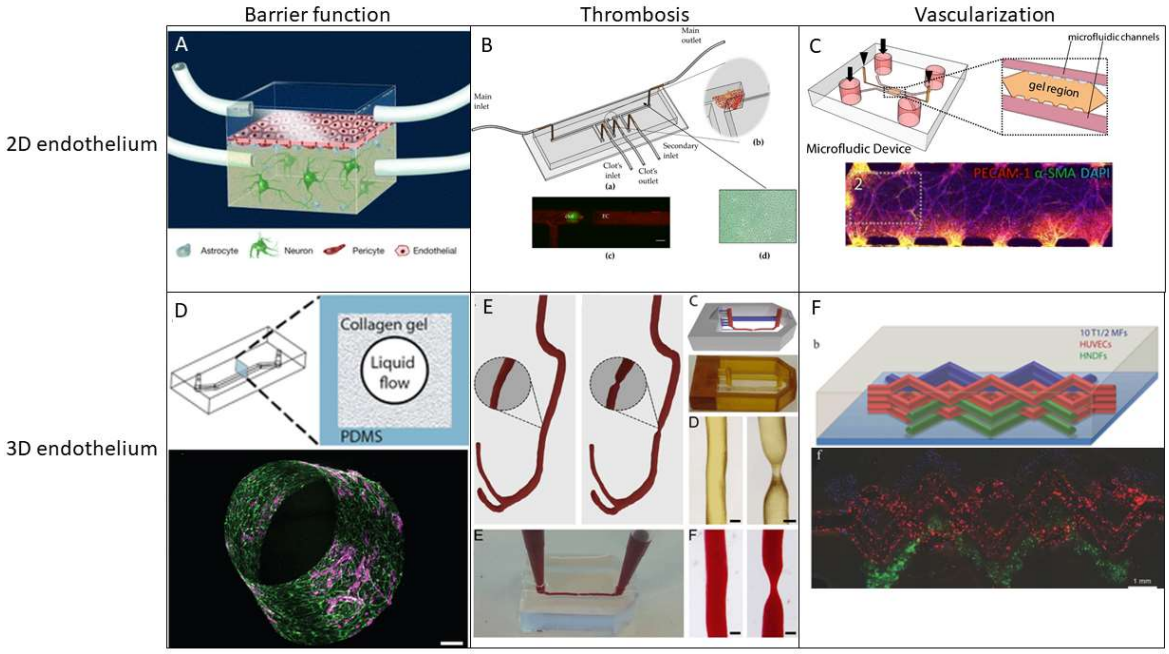

Figure 4: Overview of different blood vessels on chip. Systems are categorized in 2D (A-C) or 3D (D-F) endothelium. Chips are used to investigate the barrier function (A,D), thrombosis (B,E) or vascularization (C,F). A: 2D endothelium to simulate the blood-brain barrier after an inflammatory response [43]. B: 2D endothelium in combination with a created blood clot to simulate reperfusion after ischemia [44]. C: 2D microvascular formation in a fibrin gel [45]. D: 3D endothelium in collagen gel, used for barrier permeability measurements [46]. E: 3D endothelium in bio printed stenosis [47]. F: 3D endothelium bio printed in gelMA gel [48].

Blood vessels-on-chip create new possibilities for the measurement of endothelial dysfunction. By having a circular enclosed endothelial wall with flow, the endothelial cells can be stimulated by flowing human whole blood over the cells [47]. An activated endothelial wall will have more blood platelets stuck to the wall, which can be measured via fluorescent staining of the platelets. The supernatant of the chip be stored for measurements on secreted inflammation markers or extra cytokines [49]. Further experiments can be focused on the degradation of the endothelium by measuring the permeability of the endothelial barrier.

Several of these measurements in organs-on-chip have already been performed by other researchers for their respective field of interest. A summary of the purpose of these designs and their respective measurements is shown in Table 3. While devices have incorporated a hematologic malignancy on-chip [50], there are no known devices simulating the endothelial response in a CRS-like setting.

Table 3: Overview of organ-on-chip systems combining endothelium with an inflammatory response.

Study	Device	Endothelial cell type	Measured parameters	Remarks
Zhu et al [51]	Placenta-on-chip	Human umbilical vein endothelial cells (HUVECs)	Interleukin mRNA expression, monocyte adhesion	2D endothelial layer activated with E. coli
Sharfiri et al [52]	Foreign body reaction-on-chip	HUVECs	IL-6 concentration, monocyte flux	2D endothelial layer, peristaltic perfusion
Nemcovsky et al [44]	Ischemia-on-chip	HUVECs	ICAM-1, E-selectin concentrations	2D endothelial layer
Biglari et al [53]	Dermal inflammation-on-chip	HUVECs	Cytokine concentrations	3D vascularization grown in Matrigel
Herland et al [46]	Blood-brain barrier-on-chip	Human brain microvascular endothelial cells (hbMVECs)	Cytokine concentrations, EC permeability	3D endothelium grown on collagen matrix
Brown et al [43]	Blood-brain barrier-on-chip	hbMVECs	Cytokine concentrations, EC permeability	2D endothelial layer

The goal of this thesis is to create an organ-on-chip device to mimic the endothelial dysfunction caused by CAR-T related CRS. To model this, an *in vitro* model of the endothelium needs to be created where endothelial cells are exposed to physiological cytokine levels. The progress after this exposure can be followed by permeability assays or by measuring endothelial activation. By successfully mimicking the effects of CRS on endothelial cells, other adverse effects and their mechanisms might come to light, increasing the knowledge of CAR-T cell therapy.

Methods

To obtain the goal of a blood vessel-on-chip, multiple smaller steps had to be combined to obtain readouts from the used system. Before the system could be used, it had to be produced by casting an elastic polymer in a mould. After the polymer was cured at a high temperature, a flexible but solid slab of plastic had formed, which could be cut to size and sealed off with a microscope slide to obtain a chip with rectangular channels. These rectangular channels were prepared with chemical agents to obtain a covalent bond between the plastic and the used extracellular matrix.

A tubular channel was formed through the extracellular matrix by using a displacing liquid with a lower viscosity than the extracellular matrix. This forms an unstable interface between the two liquids, causing the low viscosity liquid to form a "finger" through the higher viscosity liquid. After the extracellular matrix and the formed channel were cured, previously expanded endothelial cells derived from stem cells could be seeded in the channel. When the cells adhered to the extracellular matrix and formed a monolayer, the cytokines from T cells and CAR-T cells could be added to the newly formed blood vessel. Their effect would then be read out by performing a permeability assay, indicating if the endothelial barrier was still intact, and immunostaining, indicating changes in cell morphology and processes in the cell. More in depth clarifications of all methods are described below in their respective subsections.

ESC-EC differentiation

Embryonic stem cells (ESCs) were provided by the Leiden University Medical Centre (LUMC). Differentiation was adapted from a previously described protocol [54], but is briefly described. After thawing, ESCs were cultured on Matrigel-coated (Corning) 6-well plates in E8 medium (Gibco), supplemented with 0.5x RevitaCell (Gibco). After 24 hours medium was replaced with BPEL medium (homemade), supplemented with 8 µM CHIR (Axon MedChem). On day three, medium was replaced with BPEL medium, supplemented with 50 ng/ml VEGF (Miltenyi) and 10 µM SB431542 (Tocris Bioscience). This medium was refreshed every three days, until endothelial cells (ECs) were isolated on day ten. Newly formed ESC-ECs were isolated using anti-CD31 Dynabeads (Invitrogen). After isolation, cells were cultured until confluent in endothelial cell serum free medium (EC-SFM; Gibco) on a 0.1% (w/v) gelatin-coated (Sigma) flask. Cells were cryo-preserved in 50% fetal bovine serum (FBS; Gibco), 40% EGM-2 medium (PromoCell), and 10% DMSO (Sigma) until further use.

Thawing and expanding of ECs

Frozen vials were thawed, then resuspended in EC-SFM supplemented with 1% platelet-poor derived serum (Biomedical Technologies), 0.6 µl/ml VEGF, and 0.2 µl/ml bFGF (Miltenyi). Resuspended cells were cultured in a 0.1% gelatin-coated 6-well plate at 13.000 cells/cm^2. Cells are grown until nearly confluent and harvested using 0.5% trypsin/EDTA (Gibco). All endothelial cells are used in the system at passage 2.

Chip fabrication

A poly (methyl methacrylate) (PMMA) mould was created using SolidWorks (Dassault Systèmes SolidWorks Corp.) and micro-milled using a CNC mill (DATRON neo). The dimensions of the channels were 10 mm x 0.5 mm x 0.5 mm (LxWxH). The mould was filled with polydimethylsiloxane (PDMS; Sylgard-184; Dow Corning) mixed 10:1 with cross linking agent. PDMS in the mould was degassed for 1 hour and placed in a 65 degrees Celsius oven for 4 hours up to overnight. Cured PDMS was removed from the mould and cut to size. Inlets and outlets were punched using a 1 mm biopsy puncher (Robbins Instruments).

22 mm x 50 mm cover glasses (Menzel) were spin coated with PDMS (5 s 500 RPM, 30 s 1500 RPM) and cured in a 65 degrees Celsius oven for 4 hours up to overnight. Cured PDMS chips and cover glasses were air plasma treated at 50 W, 66 Pa, for 40 s (Femto Science Cute) and pressed together to form a bonded chip. An example of a bonded chip is shown in Figure 5.

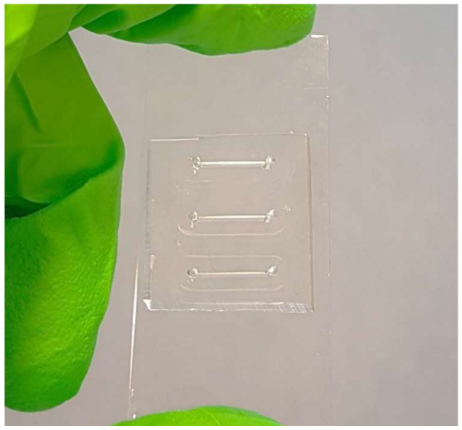

Figure 5: Bonded PDMS chip on glass cover slide. Channel dimensions: 10 mm x 0.5 mm x 0.5 mm (LxWxH).

Bonded chips were immediately treated with 3% (v/v) (3-aminopropyl)triethoxysilane (APTES; Sigma) diluted in milliQ (18.2 MΩ/cm), and incubated for 5 min at room temperature. After washing excess APTES with 70% ethanol, channels were air dried using a nitrogen flow. 10% (v/v) glutaraldehyde (Sigma) diluted in phosphate buffered saline (PBS; Gibco) was applied and incubated for 5 min at room temperature. Excess glutaraldehyde was washed away with demi water and 70% ethanol. Chips were air dried with a nitrogen flow, and placed in a 65 degrees Celsius oven overnight, until further use.

Collagen-I solution

High concentration rat tail derived collagen-I (9.3 mg/ml; Corning) was prepared to a final concentration of 5 mg/ml with a pH between 7.0 and 7.2. To obtain 120 µl mixture, a solution was made by mixing 1.5 µl 1 M sodium hydroxide (NaOH) with 12 µl 10x PBS + phenol red and 41.9 µl milliQ. This solution was carefully mixed with 64.6 µl collagen-I stock solution to create a final mixture of 5 mg/ml collagen-I, without forming air bubbles. The created mixture was spun down to remove any air pockets that did form and then kept on ice to inject into the surface treated chips.

Viscous finger patterning

This method was adapted from a previously published protocol [55]. A 7 mm cut pipette tip was placed on one side of all surface activated channels before they were moved to a 37 degrees Celsius incubator. The collagen solution was prepared fresh for a set of two chips. To start the patterning, a 200 µl pipette tip was filled with 10 µl ice-cold collagen solution and pipetted into the channel, until a meniscus formed on top of the 7 mm pipette tip, on the other side of the channel. The pipette tip was left in the inlet, and a pipette tip was filled with 1.97 µl ice-cold ECGM-2 medium. The medium was ejected, to form a droplet on the pipette tip. This droplet was smeared over the 7 mm pipette tip and got pulled through the channel, indicating that a finger had formed. After forming the lumen, each

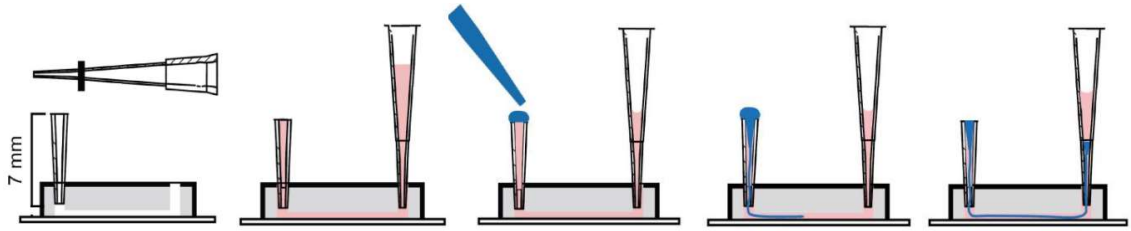

Figure 6: Schematic overview of the viscous finger patterning technique. Pink: Collagen-I solution. Blue: ECGM-2 medium. Image adapted from De Graaf et al [55].

channel was checked under the microscope to confirm the result. This process was then repeated until all chips were patterned. All chips were incubated for at least 30 minutes, to crosslink the collagen. 100 µl of warm ECGM-2 was then pipetted on top of the collagen, and the chips were placed back in the incubator overnight to further crosslink the collagen. A schematic drawing of viscous finger patterning is shown in Figure 6.

The next day, the small pipette tip was twisted and pulled from the PDMS. A new pipette tip filled with warm ECGM-2 was placed, without introducing air into the channel. This was repeated for the other pipette and chips were placed in the incubator until further use.

Cell seeding of lumens

Harvested ESC-ECs were resuspended in full ECGM-2 medium supplemented with 5 U/ml 5µg/ml penicillin/streptomycin (Pen/strep), to a concentration of $5*10^6$ cells/ml. All collagen lumens were seeded with 5 µl cell suspension, resulting in a seeding density of approximately 26.000 cells/cm^2. After adding the cells, chips were turned upside down, so cells adhered to the top of the channel, while cells were incubated for one hour. Cells were then checked under a microscope to see if they adhered. If they adhered, another 5 µl of cell suspension was added to the channels, to coat the bottom of the channel. After another hour of incubation, 100 µl of fresh ECGM-2 medium was added and cells were incubated for 4 hours up to overnight in a static state.

Afterwards, chips were either placed on a see-saw rocker in the incubator, to create a bidirectional flow over the endothelial cells, or kept in a static condition. The rocker stayed 45 seconds in each outer position, respectively +45 and -45 degrees. Chips on the rocker are shown in Figure 7. Cells are incubated on the rocker for 48 to 72 hours, refreshing medium every other day. Chips kept in a static condition were incubated for 48 to 72 hours, refreshing medium twice a day.

Figure 7: Cell-seeded chips on a see-saw rocker to create bidirectional flow. Rocker moves between +45 and -45 degrees to create a flow between the pipette tips filled with medium.

Cytokine stimulation

CAR-T cytokines were obtained from the Fraunhofer IGB, courtesy of dr. Madalena Cipriano and dr. Peter Loskill. At their institute, a tumour-on-chip device was lined with microvascular endothelial cells on a membrane and (CAR-)T cells were flushed through the first channel as depicted in Figure 8. On the other side of the membrane, the channel was filled with MDA-MB-231 (human epithelial breast cancer cell line) cancer cell spheroids embedded in a hydrogel. A schematic drawing of the chip is shown in Figure 8. Controls were performed on chip using hydrogel without cancer cells, and by comparing the cytokine release of T cells from the same donor to the cytokine release of CAR-T cells. As a control for 3D compared to 2D, T cells and CAR-T cells were also cultured separately in suspension in a 6 wells plate, without other cell types present. After 24 hours of incubation with the CAR-T cells, the media effluent was spun down to remove cells and cell debris, and frozen in a -80 degrees Celsius freezer. The frozen media was sent to Enschede and stored in a -30 degrees Celsius freezer until use.

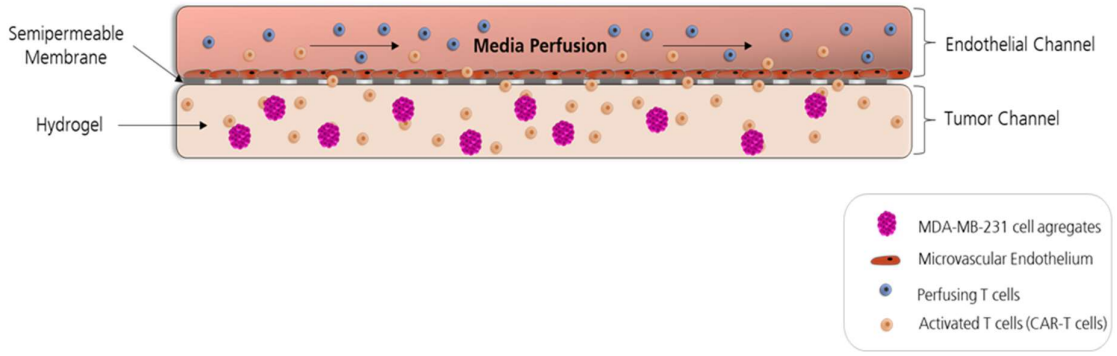

Figure 8: Schematic overview of the microphysiological tumour-on-chip that was used to create cytokine medium. A hydrogel embedded with cancer cell aggregates was cultured in combination with CAR-T cells in suspension. The CAR-T cells could permeate through the membrane into the hydrogel, killing the tumour cells. Activated CAR-T cells secreted cytokines, that dissolved in the medium. This medium was taken as effluent and sent to Enschede.

Before use, cytokines were thawed at room temperature. As a positive control, 1 ng/ml TNF-α diluted in ECGM-2 medium was used. For a negative control, the ECGM-2 medium was refreshed. A

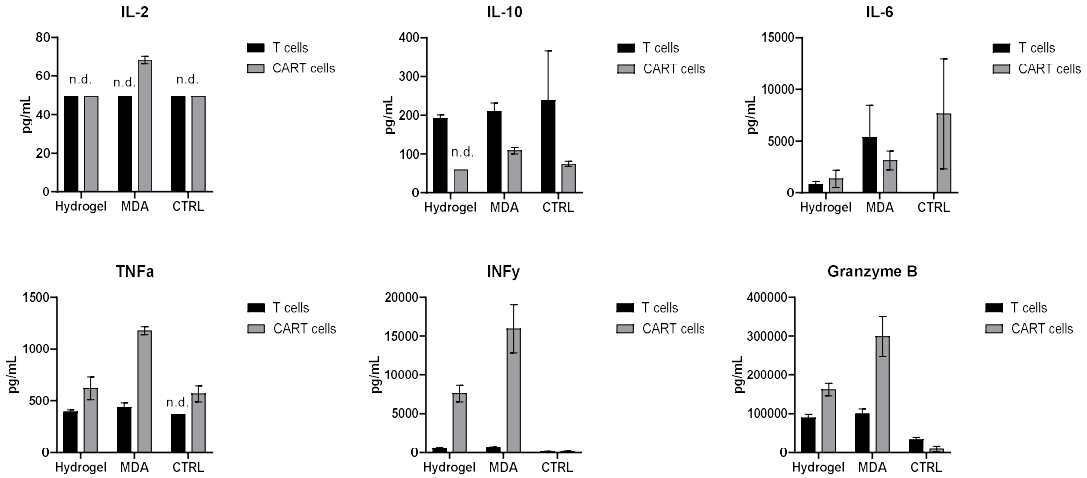

Figure 9: Characterization of taken cytokine medium divided per measured cytokine. Conditions are divided in T cells and CAR-T cells. Hydrogel is where the (CAR-)T cells circulated through the chip of Figure 8, without cancer cell aggregates present. MDA had (CAR-)T cells circulate through the chip of Figure 8, while cancer cell aggregates were present in the hydrogel. CTRL had (CAR-)T cells cultured in suspension in a 6 wells plate, without other cell types present.

characterization of a selection of the cytokines for endothelial activation secreted by CAR-T cells is shown in Figure 9.

To stimulate the cultured endothelial layers, ECGM-2 medium was removed from the endothelial cell lined lumens as much as possible, without introducing air. 100 µl of diluted cytokine medium was put in the channels and were returned to the rocker for 24 hours. After 24 hours, cytokine medium was removed from the chip and stored in Eppendorf tubes. The tubes were spun down to remove cells and cell debris and stored in a -30 degrees Celsius freezer until further analysis externally.

Fluorescent angiography

To observe the change in permeability of the endothelial barrier, fluorescent angiography was performed. Stimulated chips were connected to a syringe pump (Harvard Apparatus) that was set up to a flow rate of 25 µl/min. A pipette tip was filled with 60 µg/ml fluorescently labelled dextran (40 kDa; Invitrogen), which flows through the channels. To observe the permeability, an EVOS fluorescence microscope (Life Technologies) took photos every 10 seconds around the halfway point of the channel, monitoring the flux of fluorescent dye over the endothelial barrier.

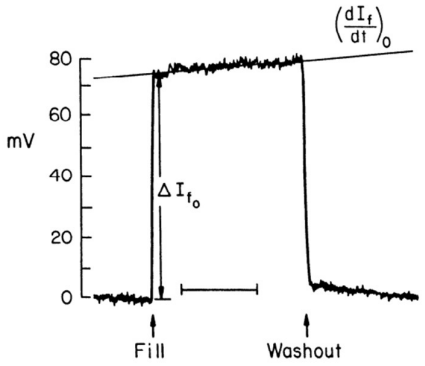

Figure 10: Example of a fluorescent angiography study outcome from Huxley et al [56]. When the dye is added in the channel, a sharp increase is measured as ΔI. Afterwards, linear growth is seen, which is deemed the flux over the endothelial barrier (dI/dt).

An example of a previously conducted fluorescent angiography study is shown in Figure 10 [56]. In this study, the first photos were taken without flow of fluorescent dye, to establish the background noise of the setup. Fluorescent dye was added, and the flow was started, which increased the initial intensity of the channel (ΔI). After this sharp increase, a linear growth was observed as the fluorescently labelled dextran permeates through the endothelial barrier into the collagen (dI). Over time the flux decreased into a sub-linear growth. The time between the initial increase and the point of sub-linear growth is measured (dt). When the pipette was almost empty it was filled with ECGM-2 medium to wash out the fluorescent dye. This created a similar pattern as with the fluorescent dextran, but with a decreasing intensity.

$$P_{app} = \frac{1}{\Delta I}\left(\frac{dI}{dt}\right)_0 \frac{r}{2} \qquad (1)$$

Images were analysed by using ImageJ [57]. The image set of a condition was loaded in as a z-stack, where the z-axis is time. The angle of the channel was measured and used to rotate the image, so the channel runs horizontally over the screen. A rectangular selection of the entire channel was made, which includes both the media channel and the crosslinked collagen. The intensity was measured of this selection, creating a dataset that was converted to MS Excel (Microsoft cooperation). A graph was created to set out the intensity over time, which was used to determine the apparent permeability (P_{app}) [56]. The used formula for P_{app} is shown in Equation 1. Value r was measured using ImageJ and

equals the radius (cm) of the lumen, measured perpendicular to the flow direction between the walls of collagen. (dI/dt) was determined by using the R^2 value between initial increase and the point of sub-linear growth. The point of sub-linear growth was determined as the point where R^2 had the highest value, with a minimum of three points between the initial growth and the sub-linear growth.

Immunostaining

A fluorescent immunostaining was performed to observe the change in cell barrier integrity, and to observe endothelial cell activation in the form of adhesion molecules. For this, stimulated channels were first treated with 4% formaldehyde (Sigma Aldrich) in PBS containing calcium and magnesium (PBS++; Gibco; v/v) for 20 minutes to fixate the state of the cells. Afterwards channels were washed twice with PBS++ and stored at 4 degrees Celsius until further treatment.

To permeate and block the cells, a solution was made of 0.1% Triton X-100 (Sigma Aldrich; w/v) and 3% bovine serum albumin (BSA; Sigma Aldrich; w/v) and incubated for 1 hour. Afterwards the channels were treated with primary antibodies, 5 µg/ml VE-cadherin (goat-anti-human; R&D systems) and 10 µg/ml ICAM-1 (Mouse-anti-human; R&D systems). VE-cadherin is a marker for tight junctions between endothelial cells and is used to visualise changes in the endothelial barrier and the morphology of cells. ICAM-1 is a protein that is used for the adhesion of immune cells to the endothelial cell and is upregulated in activated endothelial cells. Antibodies were incubated overnight at 37 degrees Celsius.

After incubation, the channels were washed with PBS++ three times to remove excess antibodies. Channels were afterwards filled with PBS++ and incubated at room temperature for 20 minutes, to leech out further excess. This incubation with PBS++ was repeated two more times, before secondary antibodies were added. Secondary antibodies consisted of 12.5 µg/ml 4',6-diamidino-2-phenylindole (DAPI) to stain the DNA, 10 µg/ml donkey-anti-goat Alexa fluor 546 (Thermo Fischer), 40 U/ml phalloidin 633 (Molecular probes). Phalloidin is used to stain the F-actin in the endothelial cells, to monitor changes in the cell morphology. The secondary antibodies were incubated for 4 hours at room temperature in a dark environment.

After incubation, the channels were washed with PBS++ three times to remove excess antibodies. Channels were afterwards filled with PBS++ and incubated at room temperature for 20 minutes, to leech out further excess. This incubation with PBS++ was repeated two more times. The last antibody was then added to prevent cross-reactivity. 2 drops/ml goat-anti-mouse Alexa fluor 488 (Invitrogen) was added to the channels and incubated for 30 minutes. The excess was washed away twice with PBS++ and chips were stored until imaging.

Stained samples were analysed with an EVOS fluorescence microscope. All images were taken at 50% intensity. The exposure time differed for each light channel but was kept the same over different conditions. The exposure time for each dye and different magnifications is shown in Table 4.

Table 4: Exposure time of each staining and magnification at 50% intensity.

	Magnification			
	4x	10x	20x	40x
ICAM-1	1000 ms	500 ms	500 ms	250 ms
DNA	120 ms	60 ms	30 ms	15 ms
Actin	750 ms	250 ms	250 ms	250 ms
VE-cadherin	750 ms	500 ms	500 ms	250 ms

Immunofluorescent analysis

Immunofluorescent images were analysed using CellProfiler [58]. A dataset of images with magnification of 20x was imported. A pipeline was then created to obtain data out of the images and the images were sorted in the categories DNA, VE-Cadherin, Actin and ICAM-1. A nucleus count is made as an indication to cell viability. To obtain a nucleus count, the pipeline first cropped the DNA images to remove part of the blurry sides of the image. Afterwards, uneven illumination was calculated by the program and corrected using a gaussian filter. Speckles were then enhanced with a white tophat filter, increasing the contrast between the nuclei and the background. This image was then processed to identify the nuclei, counting the amount per image.

Results

Viscous finger patterning

Before cells could be integrated in the system, the collagen matrix had to be formed within the channels using viscous finger patterning. Due to the multiple steps in producing lumens, a chain of mistakes could result in a failed channel. These mistakes were found and corrected over time, improving the success rate of the made channels.

Table 5: Viscous finger patterning attempts and success rates of channel formation and used channels for seeding.

Date (dd-mm-yyyy)	Total channels	Successful channels (%)	Seeded channels (% of successful)	Remarks on failed channels
02-06-2020	9	6 (66.6%)	3 (50%)	Collagen did not solidify, pH too low Bubbles in collagen mixture
18-06-2020	9	0 (0%)	-	Collagen solidified before finger was applied
22-06-2020	15	6 (40%)	-	Not enough medium for finger Collagen solidified before finger was applied
01-07-2020	9	5 (55.5%)	-	Collagen was not mixed homogeneous Collagen solidified before finger was applied
08-07-2020	9	2 (22.2%)	-	Collagen solidified before finger was applied
09-07-2020	15	11 (73.3%)	-	Collagen solidified before finger was applied
18-08-2020	18	6 (33.3%)	6 (100%)	Not enough medium for finger, micro pipette was not calibrated correctly
24-09-2020	18	13 (72.2%)	8 (61.5%)	Bubbles in collagen mixture Collagen solidified before finger was applied
07-10-2020	18	2 (11.1%)	-	Used new collagen batch Collagen was not mixed homogeneous
16-10-2020	18	18 (100%)	7 (38.9%)	-
23-10-2020	15	15 (100%)	15 (100%)	-

While any amount of collagen-I mix would suffice, as long as it filled the channel, the amount of displacing medium to create a circular channel within the collagen had to be a precise volume. This volume was tested multiple times during the manufacturing of lumens. After multiple tries, both with higher and lower volumes, the subjectively best results were obtained with 1.97 µl EGM-2 medium. Higher amounts of medium would cause a dilation of the lumen at the start of the channel, while lower amounts would not displace the collagen throughout the entire channel. Other channels could fail because of insufficient mixing of the collagen, leading to rough edges of the lumen due to a

heterogeneous composition of the collagen, or due to an overcorrection of the pH, where too much sodium hydroxide was added in the collagen mix. The success rate of the patterning attempts is shown in Table 5.

After patterning was completed, channels could still collapse or have air pockets inside the collagen. Since these effects were not created by the patterning itself, they were not taken into account in the results of successful channels in Table 5. To still give an indication, the percentage used for cell seeding is given, with 100% representing the successfully created channels after patterning. The lumens used for cell seeding are approximately 67% of the total lumens that were prepared for cell seeding.

A collection of successful and unsuccessful lumens after 24 hours of curing is shown in Figure 11. A subset of the lumens made on different occasions (n=6) was used to determine the average diameter that the lumens had. This was done by measuring the known width of the channel in ImageJ, which was used to calibrate the distance between the edges of the collagen lumen. This resulted in an average width of 320.7 ±45 µm.

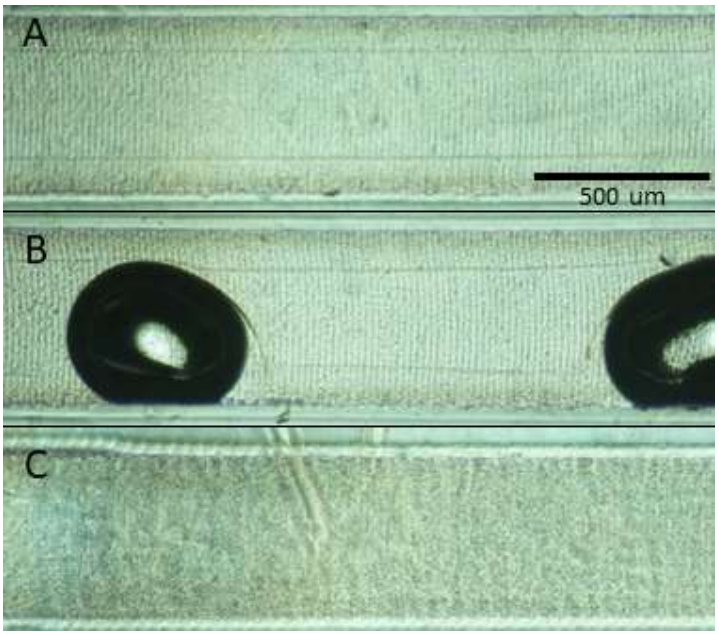

Figure 11: Lumens after 24 hours of crosslinking. A: Successful lumen with straight edges, providing an even layer for cells to adhere. B: Lumen with air bubbles that expanded from the collagen mixture. C: Lumen that did not form. The used volume to form a finger was not capable to push out the collagen mixture, creating a dense layer of collagen in the channel. Lumens were formed successfully after the used technique was optimized for personal use. Improvements could still be made to obtain a more consistent success rate in the future.

To summarize, viscous finger patterning could be used to obtain channels through an extracellular matrix of collagen-I, resulting in channels of approximately 320 µm. The success rate of forming lumens became higher as the protocol was performed more often.

Cell culturing

Human embryonic stem cell derived endothelial cells were either cultured under static conditions, where medium was refreshed twice a day, or under bidirectional flow, where medium constantly flowed over the cells while being refreshed every two days. A direct comparison between the two conditions is shown in Figure 12. Both conditions showed a monolayer that had formed after 72 hours. There were irregularities in both conditions, such as cell clumps, which did not hamper the monolayer itself.

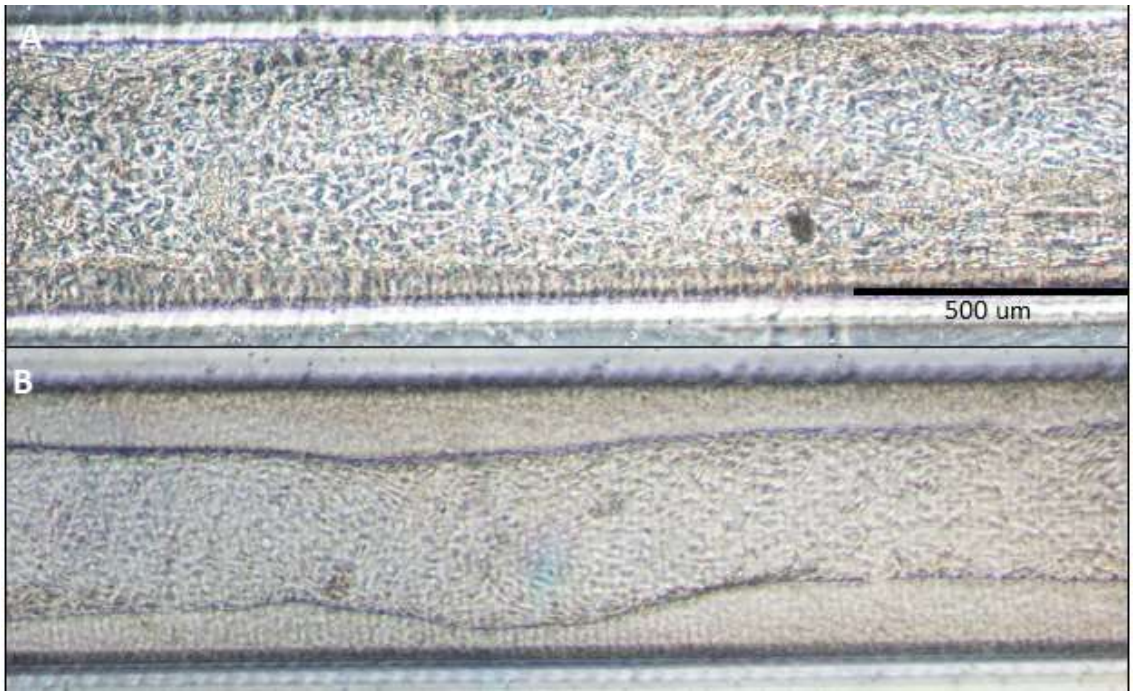

Figure 12: Morphological comparison between a lumen cultured with bidirectional flow (A) and lumen cultured under static conditions (B) after 72 hours of culture. Both channels created a monolayer without significant gaps. Cell clumps are visible in both conditions.

While both conditions did form monolayers, there were also lumens in both conditions that could not form an even monolayer. This was mainly observed right after cell seeding, where a small number of cells were on top or on the bottom of the channel. When one of the sides was not seeded sufficiently, the lumen could not be used. There were also monolayers that detached from the collagen-I lumen, creating a collapsed channel. It was not possible to perfuse such channels after the collapse, meaning that the lumen had to be discarded. Examples of lumens without an even monolayer are shown in Figure 13.

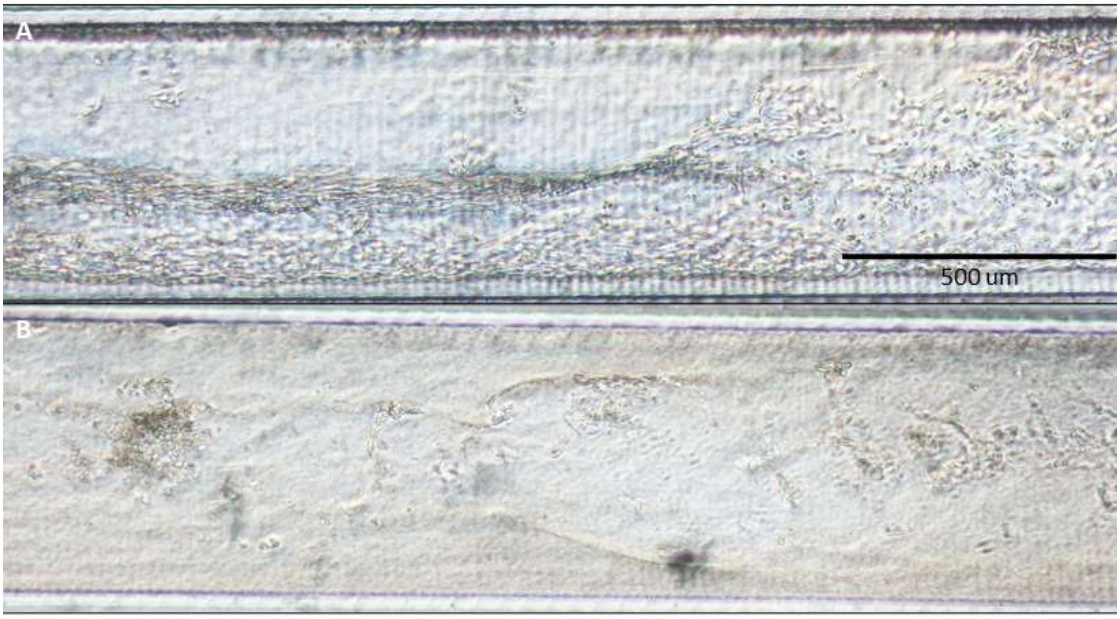

Figure 13: Examples of lumens that did not form an even monolayer. A monolayer could detach from the collagen-1 lumen (A), or not even form if the density of cells in the lumen was too low (B).

To summarize, channels could be seeded with endothelial cells, but some channels had to be discarded either due to cells pulling away from the collagen lumen, or due to a low seeding density throughout lumen.

Fluorescent angiography

The permeability was only measured on the positive and negative control conditions, which was done by performing fluorescent angiography. This was done by flushing a fluorescent dextran solution through the channel, while a time lapse was made. Using the speed at which different parameters change, equation 1 is used to calculate the apparent permeability of the endothelial barrier. A selection of time points is shown in Figure 14. Figure 14A shows an empty lumen before fluorescent dye is applied. Figure 14B shows a saturated lumen, where the fluorescent dye has permeated into the surrounding collagen. Figure 14C shows a lumen that is in the process of being washed out with medium, where the fluorescent dye slowly permeates out of the collagen. The solid blue lines show the edges of the channel, while the dashed blue lines show the edges of the collagen lumen.

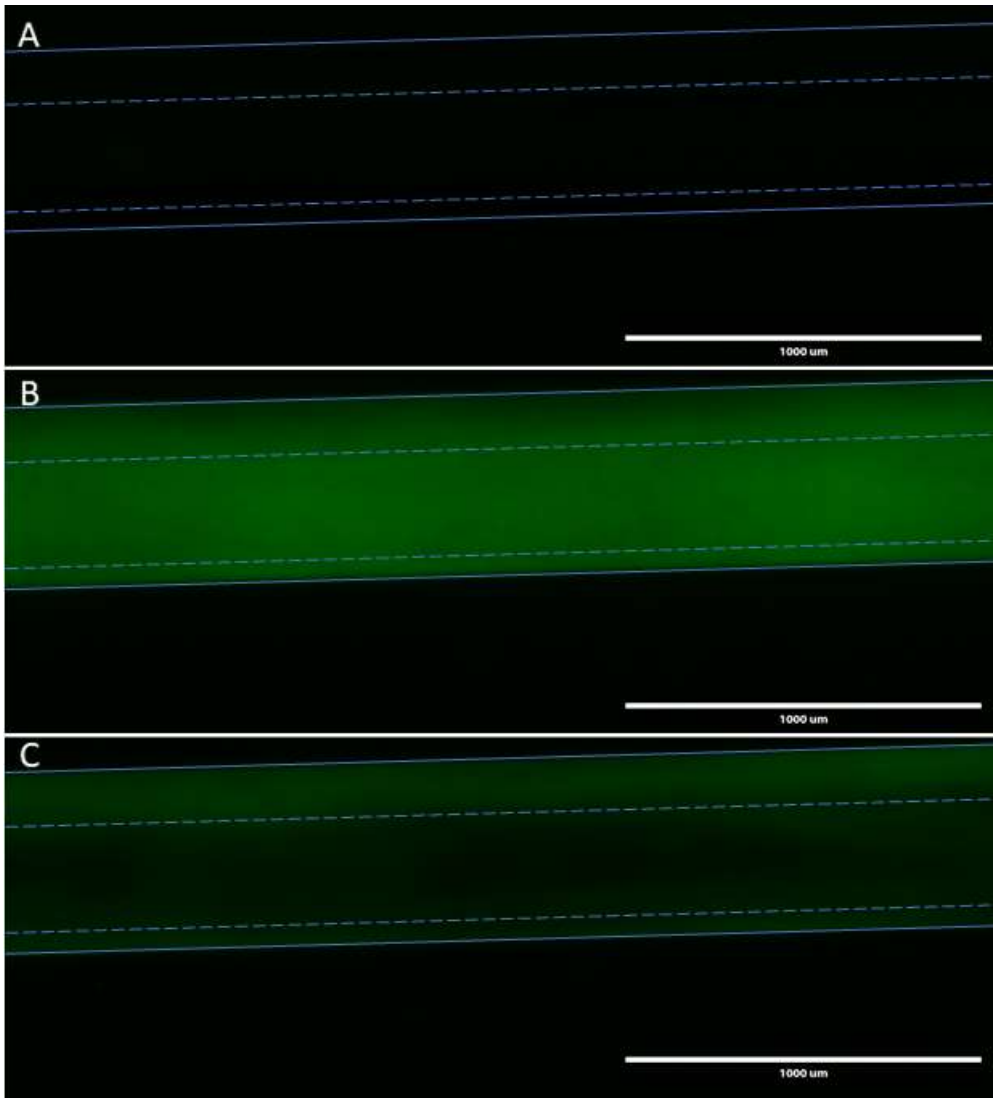

Figure 14: Fluorescent images of a lumen perfused for fluorescent angiography. A: Empty lumen before fluorescent dextran is applied. B: Lumen filled with fluorescent dextran, that has permeated into the surrounding collagen. C: Lumen filled with ECGM-2 medium that is used to flush the fluorescent dextran out of the collagen. Outer solid lines show the edges of the PDMS channel. Dashed lines show the edges of the collagen lumen.

The outer blue lines of Figure 14 were used to calculate the intensity of the area. This intensity was plotted against the total time that the permeability was measured. These plots are shown in Figure 15. Inserts A, B and C show where the images of Figure 14 were taken. The intensity plots of each condition were used to further calculate the apparent permeability. The extracted data from Figure 15 is shown in Table 6. The positive control reaches a higher intensity overall when compared to the negative control.

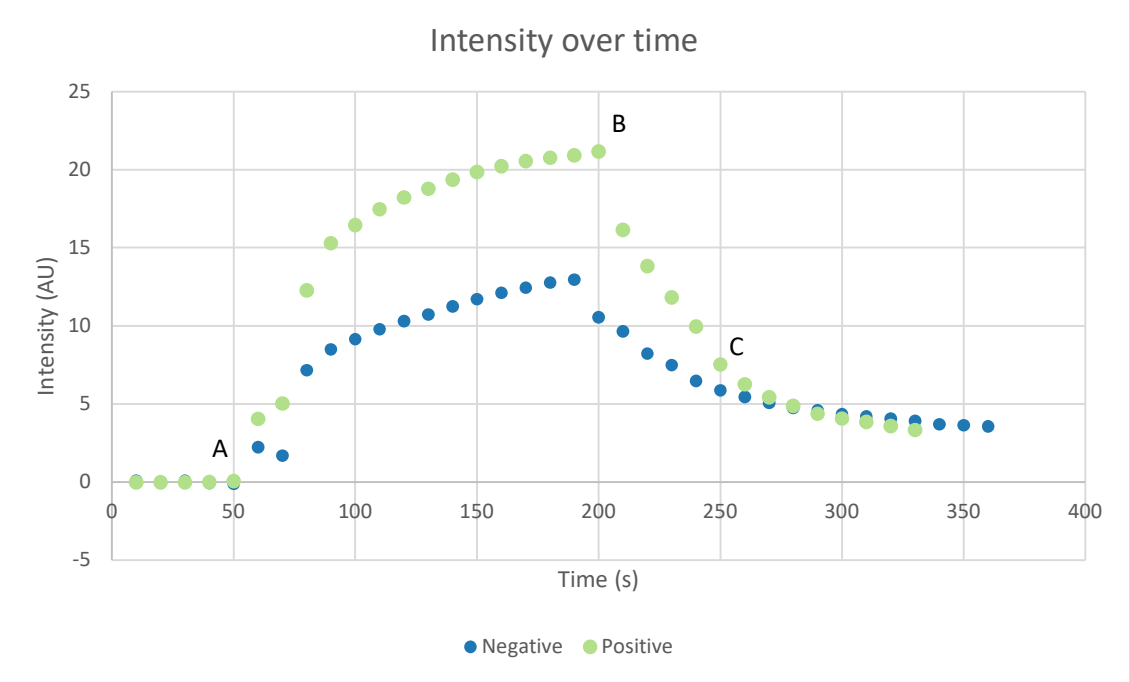

Figure 15: Intensity over time plots of the negative and positive control. The plots were used to determine the initial intensity change (ΔI) and the linear growth after the initial change (dI/dt). Inserts A, B and C show the time point of the images shown in Figure 14.

Table 6: Apparent permeability measurements taken from Figure 15.

	Positive increase	Positive decrease	Negative increase	Negative decrease
ΔI (AU)	3.9922	5.045	2.3599	2.3966
dt(s)	40	50	40	40
dI (AU)	12.4144	9.8759	6.9116	4.0984
dI/dt (1/s)	0.31036	0.197518	0.17279	0.10246
Radius (cm)	1.60E-02	1.60E-02	1.45E-02	1.45E-02
Papp (cm/s)	**1.24E-03**	**6.26E-04**	**1.06E-03**	**6.20E-04**

The measurements show that there is a difference in measuring the permeability in the fluorescent increase and fluorescent decrease. There is a small increase in permeability in the positive control when compared to the negative control. The permeability was measured once for each control, using the bidirectional flow setup.

Immunostaining

Immunostaining was performed to stain DNA, F-actin, VE-cadherin, and ICAM-1. The stainings were performed on endothelial monolayers that formed after 72 hours in the chip. Before stainings were added, cells were fixed using a formaldehyde solution. The conditions were split in T cell and CAR-T cell, which contain the conditions gel (medium from Fraunhofer tumour-on-chip without tumour cells), MDA (medium from Fraunhofer tumour-on-chip with tumour cells) and control (cells cultured in 6 wells plate without other cell types). The cytokine concentrations of these conditions were shown in Figure 9. A negative and positive control were added, which consist of respectively ECGM-2 medium and ECGM-2 medium supplemented with 1 ng/ml TNF-α.

Stainings were performed on two sets of data. The second set contained lumens that were stimulated with cytokine medium that went through an extra freeze-thaw cycle. A direct comparison of the different cytokine concentrations is shown in the Figures 16 to 22.

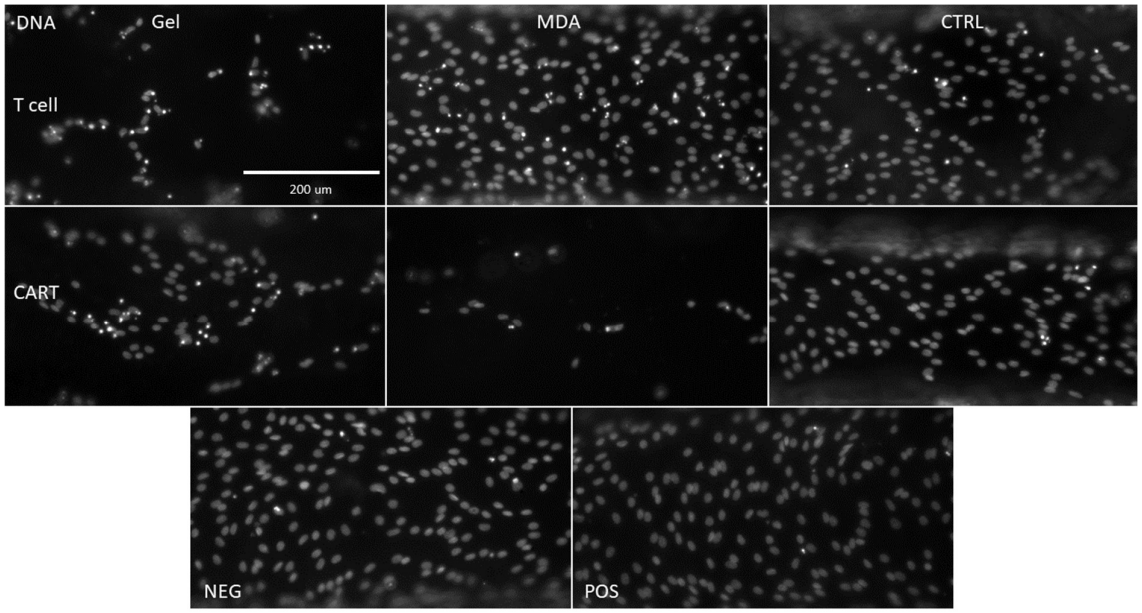

Figure 16: DNA staining of the first set of lumens. DNA staining becomes less if cells die, causing them to detach from the collagen and out of the region of interest. The staining becomes noticeably less for the conditions T cell-Gel, CART-Gel and CART-MDA. T cell: Conditions treated with medium from T cells. CART: Conditions treated with medium from CAR-T cells, derived from the same patient as the T cell condition. Gel: Conditions treated with medium from a microphysiological tumour-on-chip perfused with (CAR-)T cells, that was not filled with tumour cells. MDA: Conditions treated with medium from a microphysiological tumour-on-chip perfused with (CAR-)T cells, that was filled with MDA-MB-231 tumour aggregates. CTRL: Conditions treated with medium from (CAR-)T cells cultured in a suspension 6 wells plate, without other cell types. NEG: Condition treated with ECGM-2 medium. POS: Condition treated with ECGM-2 medium supplemented with 1 ng/ml TNF-α.

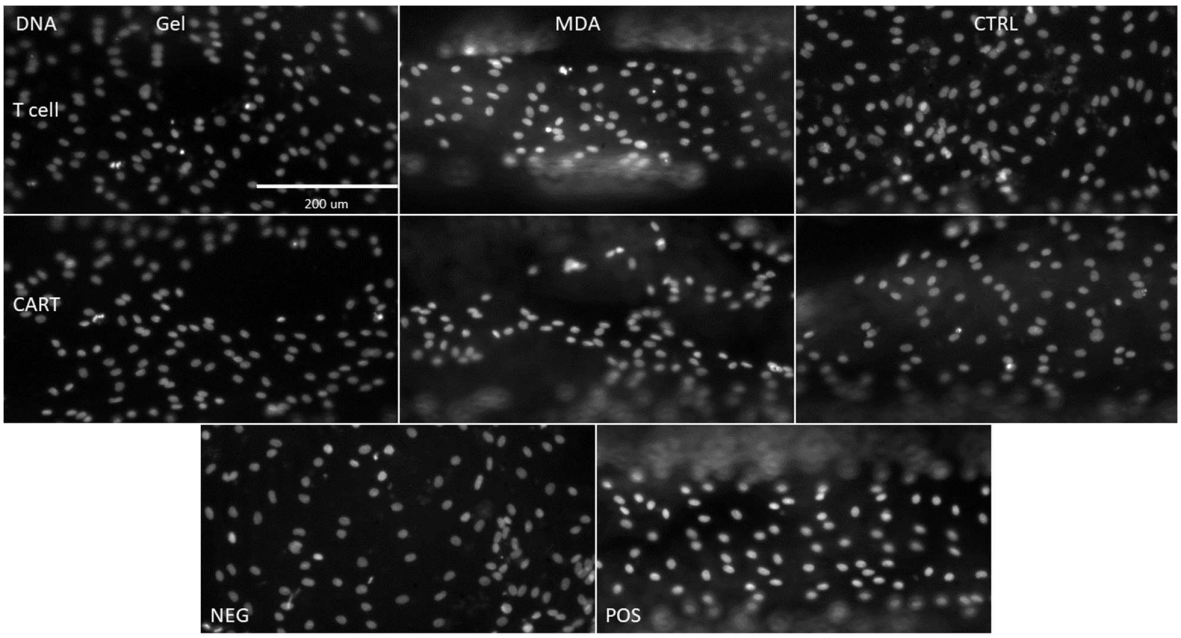

Figure 17: DNA staining of the second set of lumens. Gaps are visible in the CART-Gel and CART-MDA condition, indicating that there are no cells present in these positions. T cell: Conditions treated with medium from T cells. CART: Conditions treated with medium from CAR-T cells, derived from the same patient as the T cell condition. Gel: Conditions treated with medium from a microphysiological tumour-on-chip perfused with (CAR-)T cells, that was not filled with tumour cells. MDA: Conditions treated with medium from a microphysiological tumour-on-chip perfused with (CAR-)T cells, that was filled with MDA-MB-231 tumour aggregates. CTRL: Conditions treated with medium from (CAR-)T cells cultured in a suspension 6 wells plate, without other cell types. NEG: Condition treated with ECGM-2 medium. POS: Condition treated with ECGM-2 medium supplemented with 1 ng/ml TNF-α.

The first DNA staining set (Figure 16) shows a noticeable decrease in cells with higher cytokine concentrations. Morphologically the change is not noticeable, with conditions having the same nucleus shape in all conditions. Figure 17 shows the DNA staining of the second set of lumens, treated with cytokines that went through an extra freeze-thaw cycle. The effect that was present in the first set is less noticeable, but gaps still form in conditions with higher concentrations of cytokines.

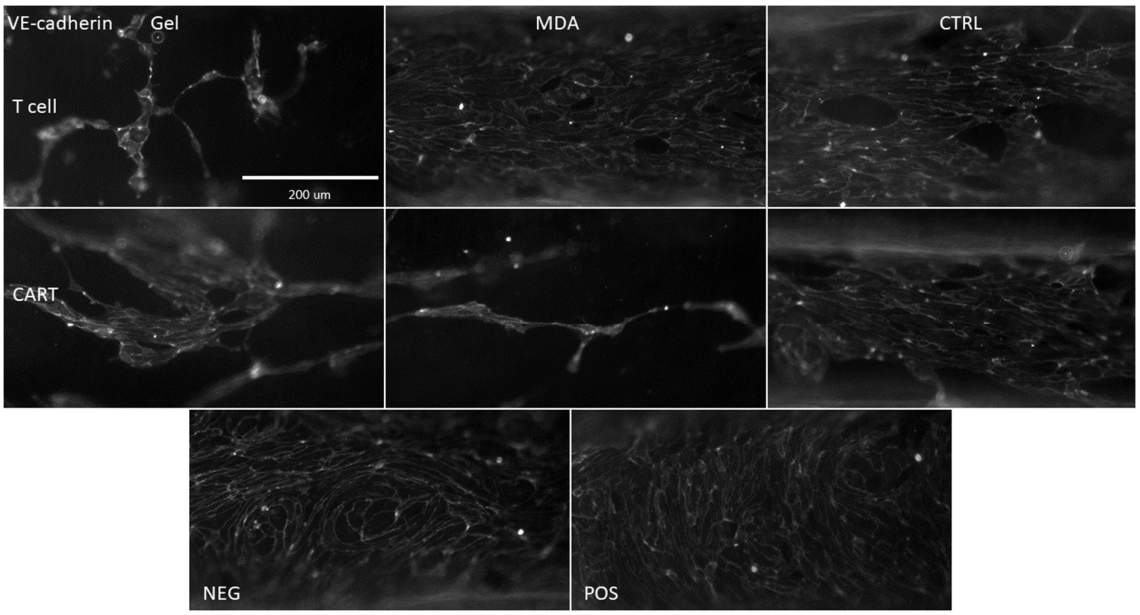

Figure 18: VE-cadherin staining of the first set of lumens. Gaps are visible in the cell monolayer in all conditions that were treated with cytokine medium, but became bigger for conditions with higher concentrations. The monolayer stayed intact for both the positive and negative control. Morphologically the VE-cadherin appears more parallel to the flow in the cytokine concentrations, when compared to the positive and negative control. T cell: Conditions treated with medium from T cells. CART: Conditions treated with medium from CAR-T cells, derived from the same patient as the T cell condition. Gel: Conditions treated with medium from a microphysiological tumour-on-chip perfused with (CAR-)T cells, that was not filled with tumour cells. MDA: Conditions treated with medium from a microphysiological tumour-on-chip perfused with (CAR-)T cells, that was filled with MDA-MB-231 tumour aggregates. CTRL: Conditions treated with medium from (CAR-)T cells cultured in a suspension 6 wells plate, without other cell types. NEG: Condition treated with ECGM-2 medium. POS: Condition treated with ECGM-2 medium supplemented with 1 ng/ml TNF-α.

VE-cadherin stains clearly show the outline of the cell monolayer in the region of interest. In the first set, shown in Figure 18, the monolayer is reduced to single cells in the T cell-Gel, CART-Gel and CART-MDA conditions. The conditions T cell-MDA, T cell-CTRL and CART-CTRL do show a larger cell sheet as monolayer, but do have gaps visible. Both the positive and negative control show a monolayer without visible gaps, but have differences in morphology. The positive control has a rough outline of the endothelial cells, whereas the negative control has a solid smooth line around the cells.

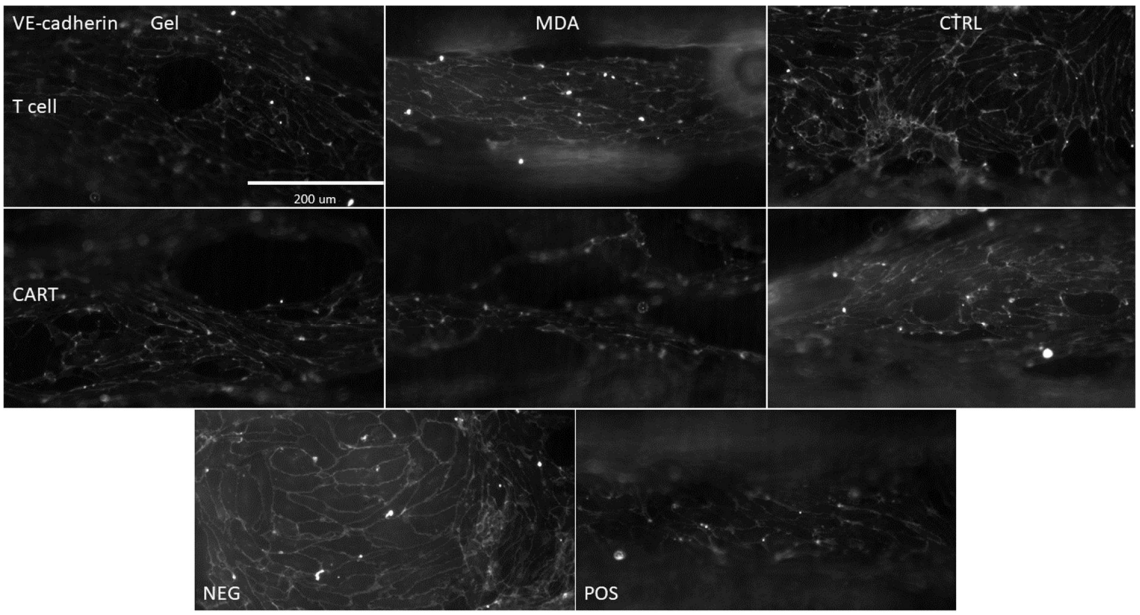

Figure 19: VE-cadherin staining of the second set of lumens. Gaps are visible in all cell monolayers stimulated with cytokine medium. The gaps become more visible in conditions with higher concentrations of cytokines. VE-cadherin morphology is more parallel in conditions treated with cytokines, but lines are thicker in the negative control. T cell: Conditions treated with medium from T cells. CART: Conditions treated with medium from CAR-T cells, derived from the same patient as the T cell condition. Gel: Conditions treated with medium from a microphysiological tumour-on-chip perfused with (CAR-)T cells, that was not filled with tumour cells. MDA: Conditions treated with medium from a microphysiological tumour-on-chip perfused with (CAR-)T cells, that was filled with MDA-MB-231 tumour aggregates. CTRL: Conditions treated with medium from (CAR-)T cells cultured in a suspension 6 wells plate, without other cell types. NEG: Condition treated with ECGM-2 medium. POS: Condition treated with ECGM-2 medium supplemented with 1 ng/ml TNF-α.

The second set of VE-cadherin staining is shown in Figure 19. This set also shows a decrease in covered lumen if the cytokine concentration is higher, similar to the first data set shown in Figure 18. The morphology of VE-cadherin appears mostly the same, where the negative control has thick and continuous lines around the cells. Conditions treated with cytokines show thinner lines and appear to be less smooth.

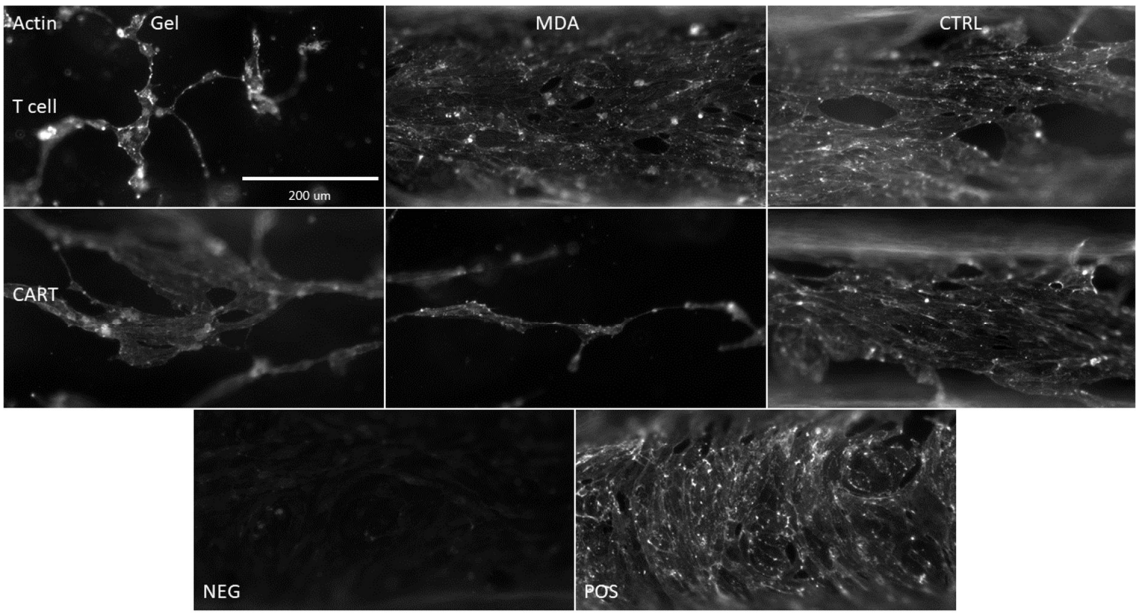

Figure 20: Actin staining of the first set of lumens. Actin filaments should appear throughout the whole cell, which helps in determining the covered area of the lumen by the cell monolayers. All conditions show dots of higher intensity in the cells, except for the negative control. The negative control has a lower intensity of the actin staining than the other conditions. T cell: Conditions treated with medium from T cells. CART: Conditions treated with medium from CAR-T cells, derived from the same patient as the T cell condition. Gel: Conditions treated with medium from a microphysiological tumour-on-chip perfused with (CAR-)T cells, that was not filled with tumour cells. MDA: Conditions treated with medium from a microphysiological tumour-on-chip perfused with (CAR-)T cells, that was filled with MDA-MB-231 tumour aggregates. CTRL: Conditions treated with medium from (CAR-)T cells cultured in a suspension 6 wells plate, without other cell types. NEG: Condition treated with ECGM-2 medium. POS: Condition treated with ECGM-2 medium supplemented with 1 ng/ml TNF-α.

The actin filament stainings, shown in Figure 20 and 21, show the cytoskeleton of the endothelial cells. The cytoskeleton is helpful in determining the covered area by the cells on the lumen, which is decreased if higher concentrations of cytokines are present. The conditions treated with cytokines in the first set show dots of higher intensity throughout the cells. This is not visible in the negative control, which has a lower intensity overall, making it difficult to see the cytoskeleton of this condition. The morphology of the actin staining is mostly the same as the morphology of the VE-cadherin stains, showing a parallel growth of the cells in cytokine stimulated conditions, while this is not the case for the positive and negative control.

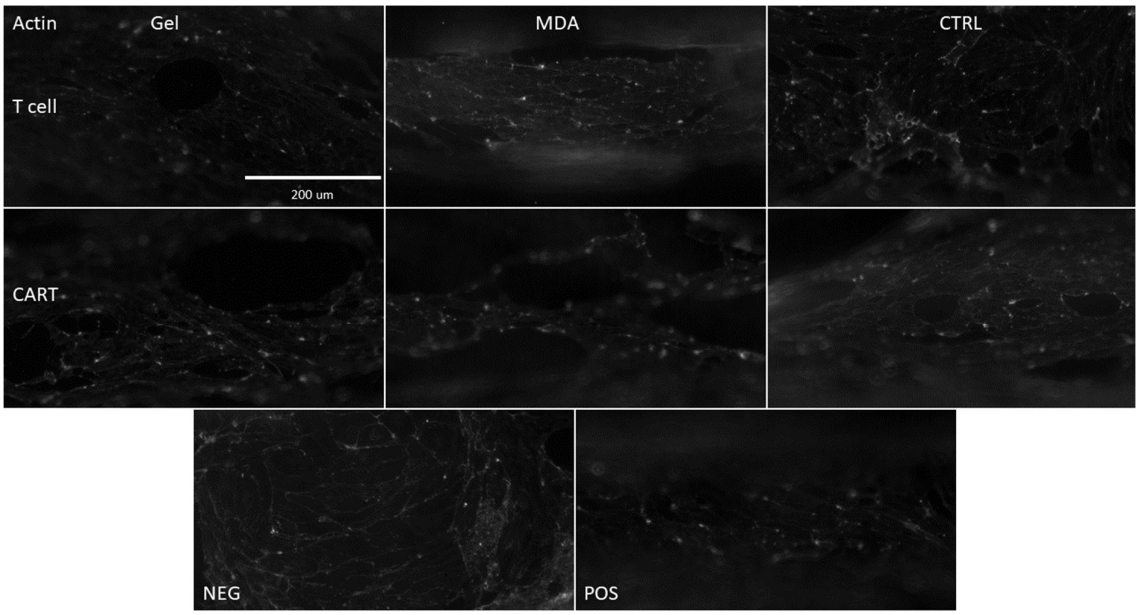

Figure 21: Actin staining of the second set of lumens. All conditions show dots of higher intensity in the cells. The negative control has a lower intensity of the actin staining than the other conditions. T cell: Conditions treated with medium from T cells. CART: Conditions treated with medium from CAR-T cells, derived from the same patient as the T cell condition. Gel: Conditions treated with medium from a microphysiological tumour-on-chip perfused with (CAR-)T cells, that was not filled with tumour cells. MDA: Conditions treated with medium from a microphysiological tumour-on-chip perfused with (CAR-)T cells, that was filled with MDA-MB-231 tumour aggregates. CTRL: Conditions treated with medium from (CAR-)T cells cultured in a suspension 6 wells plate, without other cell types. NEG: Condition treated with ECGM-2 medium. POS: Condition treated with ECGM-2 medium supplemented with 1 ng/ml TNF-α.

The ICAM-1 staining was only performed on the first set of lumens and is depicted in Figure 22. The outline of the cells is visible in conditions with a relatively high concentration of cytokines, like T cell-Gel, CART-Gel, and CART-MDA. In the other conditions there is no visible staining of cells for ICAM-1.

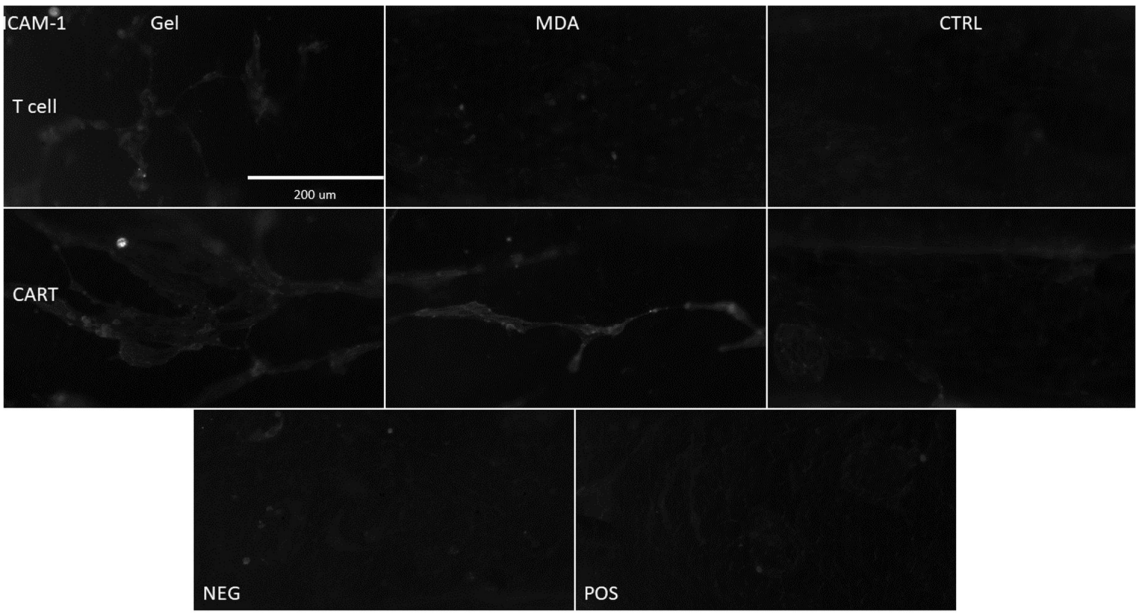

Figure 22: ICAM-1 staining of the first set of lumens. A clear outline of the cells is seen in conditions with higher concentrations of cytokines, like T cell-Gel, CART-Gel and CART-MDA. Control conditions show no visible immunostaining for ICAM-1. T cell: Conditions treated with medium from T cells. CART: Conditions treated with medium from CAR-T cells, derived from the same patient as the T cell condition. Gel: Conditions treated with medium from a microphysiological tumour-on-chip perfused with (CAR-)T cells, that was not filled with tumour cells. MDA: Conditions treated with medium from a microphysiological tumour-on-chip perfused with (CAR-)T cells, that was filled with MDA-MB-231 tumour aggregates. CTRL: Conditions treated with medium from (CAR-)T cells cultured in a suspension 6 wells plate, without other cell types. NEG: Condition treated with ECGM-2 medium. POS: Condition treated with ECGM-2 medium supplemented with 1 ng/ml TNF-α.

Further analysis of the immunostainings of the DNA was done in CellProfiler. A pipeline was created to identify the nuclei in each condition, by counting the 'objects' in the DNA images. The nucleus count is deemed as an indicator for the cell viability in each condition. If there are more nuclei counted, the monolayer should be more intact in that region of interest. This count is shown in Figure 23. As a comparison between T cells and CAR-T cells, the counted nuclei are lower in conditions treated with CAR-T cell medium. The positive control has a lower nucleus count than the negative control.

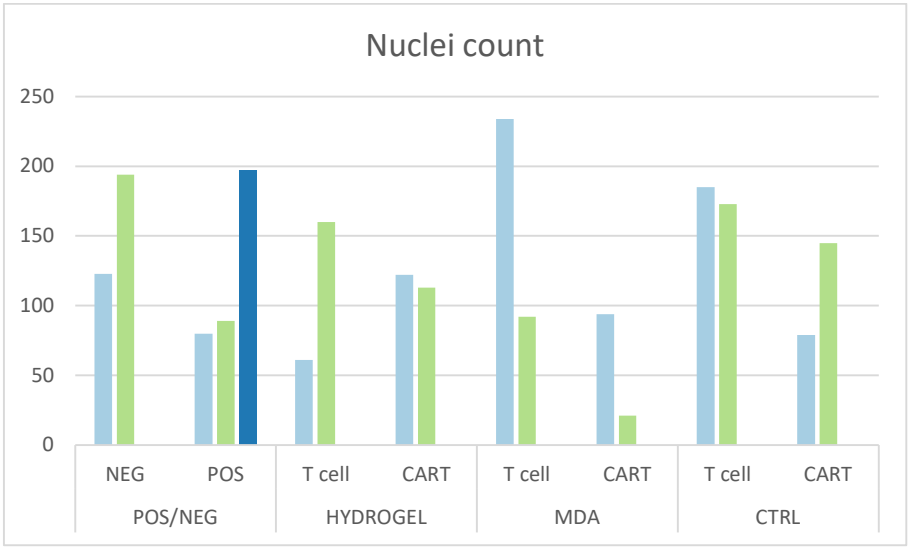

Figure 23: Nuclei count of the images in Figure 16 and 17. A decrease in nuclei counted is deemed as a destruction of the monolayer. If there are more cells present, more nuclei should be counted. T cell: Conditions treated with medium from T cells. CART: Conditions treated with medium from CAR-T cells, derived from the same patient as the T cell condition. Gel: Conditions treated with medium from a microphysiological tumour-on-chip perfused with (CAR-)T cells, that was not filled with tumour cells. MDA: Conditions treated with medium from a microphysiological tumour-on-chip perfused with (CAR-)T cells, that was filled with MDA-MB-231 tumour aggregates. CTRL: Conditions treated with medium from (CAR-)T cells cultured in a suspension 6 wells plate, without other cell types. NEG: Condition treated with ECGM-2 medium. POS: Condition treated with ECGM-2 medium supplemented with 1 ng/ml TNF-α.

The immunostainings show that there is a change in morphology for VE-cadherin, Actin, and ICAM-1 if cytokines are applied to the endothelial cells. After analysis of the DNA images in CellProfiler, it is shown that there is a decrease in nuclei if CAR-T cells are used instead of T cells.

Discussion

In summary, the results showed the formation of collagen lumens using viscous finger patterning. These lumens were seeded using human embryonic stem cell derived endothelial cells to create a monolayer of endothelial cells. The effect of (CAR-)T cell derived cytokines was determined using fluorescent angiography and immunostaining. The fluorescent angiography showed a proof of principle for the measurement of more conditions, while the immunostaining showed that there is a decrease in cell viability if the cytokine concentration is higher. These results are further analysed, discussed, and compared to previous literature, giving an insight in the relevancy of microphysiological systems to discover adverse effects during pre-clinical trials.

Viscous finger patterning

During preparation of the collagen lumens there was an increase in success rate over time. This was mainly attributed to better knowledge of how the collagen behaved, which also explains the drop off in success when a new batch was used for the first time. The main contributor to failing channels was that the collagen solidified before the medium could form a finger through the collagen. Two possible reasons why this happened were either a wrong balance in the collagen master mix, or a longer period of spinning down the collagen to remove air bubbles.

The target value of the pH for the collagen mixture was 7.0-7.2. When the pH was too low after initial mixing, a small amount of NaOH was added by dipping a 10 µl pipette first in a 1 M sodium hydroxide mixture and then in the collagen mixture. Since the collagen mixture had a volume of only 120 µl, a very small excess of NaOH could change the pH from slightly acidic to very basic, overshooting the target value. Since this is also a step which could take some time, mainly due to the extra mixing required to reobtain a homogeneous mixture, this could mean that the collagen started to cross link while still in the Eppendorf tube [59]. This same problem could happen when the collagen was spun down too long to remove air bubbles. The extra time could have been long enough for the collagen to start the initial cross linking, increasing the viscosity of the channel to such a degree that the medium finger could not move through the block.

The cross-linking time is increased if all required materials are kept at a low temperature. However, this is at a balance with any possible air bubbles that can arise in the system. To keep the growth of air bubbles at a minimum, all materials should be kept at the same temperature. This is currently impossible because the collagen channels polymerize in a 37 degrees Celsius incubator. Therefore, a small air bubble created due to mixing, can grow in a large air pocket within the collagen, destroying the lumen [60]. Careful mixing is therefore required, but was not always reached, further limiting the production process.

The created collagen lumens had a measured diameter of 320 ±45 µm. The diameter of the lumen could vary within a channel but was not deemed as a problematic observation to discard the channel. The overall diameter of a formed lumen is dependent on the dimensions of the rectangular channel and the viscosity of the displacing and displaced liquid [46]. Other papers that are using the same channel diameter of 10 mm x 0.5 mm x 0.5 mm (LxWxH), obtain diameters of 261 ±28 µm [55] and 256 ±21 µm [61]. Differences could be explained by variations in liquid viscosity due to differing concentrations of collagen-I, or by the time that the collagen sat in the channel before medium was used as a finger.

Cell culturing

Both methods of perfusing the cells did form monolayers with small irregularities. While they looked similar when observed using light microscopy, there might have been differences in the monolayer density regarding intracellular junctions, since an applied flow leads to a tighter monolayer where endothelial cells block more molecules [62]. If a monolayer is formed through the entire channel, this difference in cell-cell contacts could lead to a difference in permeability.

During cell seeding a common occurrence was the heterogeneity of the cell seeding mixture. All lumens in a batch were seeded with the same cell mixture of $5.0*10^6$ cells/ml. While the cell mixture was resuspended before every seeding step, there were still channels with a lower cell density than others. Since the cells were mixed and pipetted using a narrow gel loading tip, it is possible that the pipette created a jetting stream in the Eppendorf tube, failing to create a homogeneous mixture of cells. Tapping the side of the Eppendorf tube more vigorously could help here if used in combination with the gel loading tips, which would in turn lead to a constant higher success rate of lumens with a monolayer.

Cytokine stimulation

The cytokines obtained from the Fraunhofer IGB were sent as triple duplicates. The cytokines in these duplicates were measured via ELISA, and their results were presented in Figure 9. These results were the average measurement of the duplicates, with error bars to fit all three measurements. This means that the exact concentration of cytokines was not known for each of the vials, which could lead to differences in the same conditions, as a different vial had to be used for each experiment.

Since more than three experiment sets were run on the endothelial cells, the cytokine medium eventually had to be thawed a second time for use. This extra freeze-thaw cycle might have had an effect on the cytokine concentrations, as not all cytokines are stable during temperature changes [63]. This can be avoided by creating smaller aliquots of cytokine medium before they are frozen at the Fraunhofer IGB, since only 100 µl of cytokine medium is used for each channel.

Cytokines that were harvested from the endothelial lumens after 24 hours of incubation were not yet analysed to monitor changes in the cytokine concentrations. It is expected following literature that the endothelial cells help in the secretion of cytokines, if they are stimulated with cytokines secreted by immune cells [7]. This hypothesis will be tested in later stages since experiments are still ongoing.

Fluorescent angiography

Measuring the fluorescent angiography was prone to user error during both the observation of fluorescent dye using the microscope and during the data analysis. The dye was applied with a gel loading tip into a cut pipette tip that was inserted in the chip. This application had to be done in between two images, which were 10 seconds apart. If this was not done quick enough, a data point had an increase of intensity that was not in line with the rest of the graph. Since fluorescent dye might already have flowed through the chip at this point, the initial increase was then lost in the background signal. If this was done correct, the ΔI of increase and decrease should be approximately the same value. The occurrence of this error might decrease as the user gains more experience with the procedure, leading to a more robust measurement.

The data analysis was done by observing the data points in Excel. After the initial increase or decrease, the linear growth was measured until sub-linear growth was reached. This was done by plotting only the linear growth against time in a separate graph. Data points were added until the R^2 value reached its maximum value, or until a point went under or over the linear trend, for the increase and decrease

respectively. A script could be created to fit the sublinear graph to a linear function, with set data points to distinguish where the plot derivates too much from the linear trend to be deemed linear.

The technique of fluorescent angiography and the function to calculate the permeability in this study assume that the endothelial barrier is the only barrier contributing to the permeability. This assumption does not include the existence of larger gaps between the cells, where the collagen acts as the main barrier for molecules to permeate. By increasing the size of the used fluorescent dye, the assumption could be closer to what is measured during the experiment. Larger molecules would be blocked by the endothelial barrier for a longer time, increasing the linear trend of the fluorescence over time.

The measured conditions did not obtain a large difference in the permeability value, where both conditions have values between $0.5*10^{-3}$ and $1.5*10^{-3}$ cm/s. When compared to literature, a monolayer of endothelial cells should have an apparent permeability that is closer to values between $1.0*10^{-6}$ and $1.0*10^{-5}$ cm/s [46], [64], [65]. This means that a monolayer was not established in both conditions, so more tests must be performed with a more robust method to obtain a monolayer. When a monolayer can be established with a negative control, the barrier function can be disrupted with the cytokines to obtain measurements for the conditions.

Immunostaining

Immunostaining was performed on two occasions to stain the effects of the cytokines on endothelial cell activation and barrier function. Endothelial cell activation was linked to staining the cells for ICAM-1, a protein stimulating the adhesion of white blood cells, while the barrier function was linked to the expression of VE-cadherin, which is a protein for intra-cellular junctions. To compare differences within a set, all fluorescent images were taken at the same exposure time and light intensity. The images had some blurs near the top and bottom, due to the geometry of the lumen. The images could be improved by taking another set of images with a confocal microscope, which can make scans of multiple planes over the z-axis, stitching them together for a sharp image in all planes.

While the conditions between sets can be compared, it is not possible to quantify the measurements of the sets to one another. The second set of immunostaining images was obtained after stimulation using cytokine media that went through an extra freeze-thaw cycle, which explains why the data has a more intact layer of cells when compared to the first set. The image sets both show that cells decrease under conditions with a higher amount of granzyme B, like CART-MDA, T cell-Gel and CART-Gel. This decrease of cells is quantified by the nucleus count.

Immunostaining of stimulated endothelial cells must be further tested for the ICAM-1 measurement. While there seems to be an increase in its intensity for conditions where an upregulation of ICAM-1 is expected, it is not clear whether this increase is specifically bound to the ICAM-1 protein or if it is autofluorescence of the cell. Literature shows that endothelial cells show clusters of ICAM-1 when activated by cytokines such as TNF-α [66]. This is not the case in the ICAM-1 stains shown in Figure 22, where cells are stained throughout if there is a signal. Better understanding of the antibody might be obtained by performing an optimization of 1^{st} and 2^{nd} antibodies concentration on endothelial cells cultured in a 2D monolayer.

The morphology of the VE-cadherin staining is expected to change when cytokines are applied. Literature states that VE-cadherin is “abnormally distributed” and expression decreases if the endothelial barrier is disrupted [67]. Abnormal distribution is classified as an interrupted VE-cadherin line around the cell, with reduced expression. Monolayers with normal distributed VE-cadherin should show as a continuous line between endothelial cells. In the images shown in Figure 18 and 19, VE-

cadherin expression does become thinner with the application of cytokines. An interrupted line could not be found, but this could also be contributed to the low number of cells that is left in conditions with high concentrations of cytokines, like CART-MDA.

The nuclei count performed with CellProfiler shows that overall there is a decrease of cells when CAR-T cells are compared to T cells. When compared to the cytokine concentrations in Figure 9, this was expected since the CAR-T cells produce more cytokines than the T cells. The higher concentration of cytokines shows that the CAR-T cells at the Fraunhofer IGB were specifically activated by their tumour-on-chip. The nuclei count within the same condition has a high difference since a second set was performed with cytokines that went through an extra freeze-thaw cycle. When the data is compared within the same set, a decrease is visible for almost all conditions. The only condition with approximately the same nuclei count is the hydrogel. A better comparison of this condition could be made if the cell count was performed on more samples, since the count of CART-Gel falls between the two outer counts of T cell-Gel.

Use of microphysiological systems for pre-clinical trials

While other microphysiological systems with endothelial cells make use of cytokines to disrupt the barrier function to model their respective disease, this system is the first model for CAR-T cell mediated CRS. Models currently in place to assess new CAR-T therapies often make use of animal models or simple *in vitro* petri dish models, so more advanced models could help with a better translation from pre-clinical trials to early phase clinical trials [68].

The model currently used in this study consists of two separate organs-on-chips that are connected by manual handling of cell culture media. Further development of the model could integrate the two models together, creating a circular flow from the Fraunhofer tumour-on-chip system to the endothelium lumen, back to the tumour-on-chip. This would decrease limitations of transport of the medium, while also increasing the physiological relevance of the chip.

One CAR-T therapy was shut down while in phase 2 clinical trials, due to five cases of fatal adverse effects [69]. While the investigation is ongoing, better understanding of CAR-T therapies and their adverse effects is still needed. This is not only the case for CAR-T cell therapies, but also for other T cell-based immunotherapies. Early trials with a CD28 receptor based antibody (TGN1412) were shut down in phase 1 after the drug caused CRS in all volunteers [70]. After investigation it was deemed that this could have been avoided if better models were in use during the pre-clinical trial.

Using microphysiological systems to understand the interaction between CAR-T cells and the endothelium could give insights to the adverse effects that were found in earlier conducted clinical trials. The current system would need improvements to mimic the CRS- endothelium interaction that is found *in vivo*.

Future outlook

The negative control must become a better representation of a healthy endothelium, by improving the methods to obtain an even monolayer throughout the chip. Furthermore, there is a need for a more subtle response to the cytokines currently used, so there will not be a full breakdown of the endothelium. This subtlety could be created by diluting the cytokines or by having a shorter incubation time. Further improving the system by performing perfusion with whole blood could lead to a more complete immune reaction of the endothelium, where coagulation disorders can be monitored [47].

Conclusion

To conclude, a microphysiological system was used to mimic the effects of CAR-T mediated CRS on endothelial cells. The results of the fluorescent immunostaining provide a proof of concept that the reaction can be mimicked using the proposed methods, with a decline of cells when cytokine rich medium is applied. The fluorescent angiography assay shows that changes in permeability can be measured, if a tighter monolayer is formed for the negative control. Changes in between conditions with T cells compared to CAR-T cells could be measured in the feature, if a more subtle reaction is created using their respective cytokines. If the microphysiological system manages to mimic the effects of CRS on the endothelium it could contribute to the understanding of CRS and how to combat it in future patients.

Acknowledgements

Special acknowledgements go out to Andries van der Meer and Laura de Heus for their expertise and support on a daily basis during this internship. While the entire time spend on the thesis was dominated with working around measurements against COVID-19, their look onto things helped push me in the right direction. Also, a thank you to Jim Koldenhof, Yusuf Arik, and Anke Vollertsen. Their knowledge of the chip and discussions on how to perform certain steps in the lab helped significantly in increasing the success rate of chip fabrication. Finally, a thank you to Peter Loskill, Madalena Cipriano, and Ibrahim Maulana of the Fraunhofer IGB. They performed all experiments prior to the stimulation that is performed here and provided helpful discussions with preliminary results, contributing to the road map of microphysiological systems and CAR-T therapy.

References

[1] M. Köhler *et al.*, "Current developments in immunotherapy in the treatment of multiple myeloma: Immunotherapy in Multiple Myeloma," *Cancer*, vol. 124, no. 10, pp. 2075–2085, May 2018, doi: 10.1002/cncr.31243.

[2] "Home - ClinicalTrials.gov." https://clinicaltrials.gov/ct2/home (accessed Jul. 08, 2020).

[3] D. Abate-Daga and M. L. Davila, "CAR models: next-generation CAR modifications for enhanced T-cell function," *Molecular Therapy - Oncolytics*, vol. 3, p. 16014, 2016, doi: 10.1038/mto.2016.14.

[4] T. R. Abreu, N. A. Fonseca, N. Gonçalves, and J. N. Moreira, "Current challenges and emerging opportunities of CAR-T cell therapies," *Journal of Controlled Release*, vol. 319, pp. 246–261, Mar. 2020, doi: 10.1016/j.jconrel.2019.12.047.

[5] A. Shimabukuro-Vornhagen *et al.*, "Cytokine release syndrome," *J Immunother Cancer*, vol. 6, no. 1, p. 56, Dec. 2018, doi: 10.1186/s40425-018-0343-9.

[6] K. A. Hay *et al.*, "Kinetics and biomarkers of severe cytokine release syndrome after CD19 chimeric antigen receptor-modified T-cell therapy," *Blood*, vol. 130, no. 21, pp. 2295–2306, 23 2017, doi: 10.1182/blood-2017-06-793141.

[7] S. S. Neelapu *et al.*, "Chimeric antigen receptor T-cell therapy — assessment and management of toxicities," *Nature Reviews Clinical Oncology*, vol. 15, no. 1, Art. no. 1, Jan. 2018, doi: 10.1038/nrclinonc.2017.148.

[8] J. N. Brudno and J. N. Kochenderfer, "Recent advances in CAR T-cell toxicity: Mechanisms, manifestations and management," *Blood Reviews*, vol. 34, pp. 45–55, Mar. 2019, doi: 10.1016/j.blre.2018.11.002.

[9] N. Frey and D. Porter, "Cytokine Release Syndrome with Chimeric Antigen Receptor T Cell Therapy," *Biology of Blood and Marrow Transplantation*, vol. 25, no. 4, pp. e123–e127, Apr. 2019, doi: 10.1016/j.bbmt.2018.12.756.

[10] Z. Wang and W. Han, "Biomarkers of cytokine release syndrome and neurotoxicity related to CAR-T cell therapy," *Biomarker Research*, vol. 6, no. 1, p. 4, Jan. 2018, doi: 10.1186/s40364-018-0116-0.

[11] H. H. Yiu, A. L. Graham, and R. F. Stengel, "Dynamics of a Cytokine Storm," *PLOS ONE*, vol. 7, no. 10, p. e45027, okt 2012, doi: 10.1371/journal.pone.0045027.

[12] J. Gust *et al.*, "Endothelial Activation and Blood–Brain Barrier Disruption in Neurotoxicity after Adoptive Immunotherapy with CD19 CAR-T Cells," *Cancer Discov*, vol. 7, no. 12, pp. 1404–1419, Dec. 2017, doi: 10.1158/2159-8290.CD-17-0698.

[13] H. Jiang *et al.*, "Improving the safety of CAR-T cell therapy by controlling CRS-related coagulopathy," *Ann Hematol*, vol. 98, no. 7, pp. 1721–1732, Jul. 2019, doi: 10.1007/s00277-019-03685-z.

[14] B. G. Chousterman, F. K. Swirski, and G. F. Weber, "Cytokine storm and sepsis disease pathogenesis," *Semin Immunopathol*, vol. 39, no. 5, pp. 517–528, Jul. 2017, doi: 10.1007/s00281-017-0639-8.

[15] R. Sackstein, T. Schatton, and S. R. Barthel, "T-lymphocyte homing: an underappreciated yet critical hurdle for successful cancer immunotherapy," *Laboratory Investigation*, vol. 97, no. 6, Art. no. 6, Jun. 2017, doi: 10.1038/labinvest.2017.25.

[16] C. C. Kirwan, C. N. McCollum, G. McDowell, and G. J. Byrne, "Investigation of Proposed Mechanisms of Chemotherapy-Induced Venous Thromboembolism: Endothelial Cell Activation and Procoagulant Release Due to Apoptosis," *Clinical and Applied Thrombosis/Hemostasis*, Mar. 2015, doi: 10.1177/1076029615575071.

[17] N. Bouchkouj *et al.*, "FDA Approval Summary: Axicabtagene Ciloleucel for Relapsed or Refractory Large B-cell Lymphoma," *Clin Cancer Res*, vol. 25, no. 6, pp. 1702–1708, Mar. 2019, doi: 10.1158/1078-0432.CCR-18-2743.

[18] J. Gust *et al.*, "Glial injury in neurotoxicity after pediatric CD19-directed chimeric antigen receptor T cell therapy," *Annals of Neurology*, vol. 86, no. 1, pp. 42–54, 2019, doi: 10.1002/ana.25502.
[19] K. Stahl *et al.*, "Extracorporeal cytokine removal in severe CAR-T cell associated cytokine release syndrome," *Journal of Critical Care*, vol. 57, pp. 124–129, Jun. 2020, doi: 10.1016/j.jcrc.2020.02.010.
[20] H. Jia *et al.*, "Haploidentical CD19/CD22 bispecific CAR-T cells induced MRD-negative remission in a patient with relapsed and refractory adult B-ALL after haploidentical hematopoietic stem cell transplantation," *Journal of Hematology & Oncology*, vol. 12, no. 1, p. 57, Jun. 2019, doi: 10.1186/s13045-019-0741-6.
[21] H. Liu *et al.*, "Coexistence Of A Huge Venous Thromboembolism And Bleeding Tendency In Cytokine Release Syndrome During CAR-T Therapy," *Onco Targets Ther*, vol. 12, pp. 8955–8960, Oct. 2019, doi: 10.2147/OTT.S223697.
[22] J. Gauthier and C. J. Turtle, "Insights into cytokine release syndrome and neurotoxicity after CD19-specific CAR-T cell therapy," *Current Research in Translational Medicine*, vol. 66, no. 2, pp. 50–52, May 2018, doi: 10.1016/j.retram.2018.03.003.
[23] C. J. Turtle *et al.*, "CD19 CAR–T cells of defined $CD4^+$:$CD8^+$ composition in adult B cell ALL patients," *J Clin Invest*, vol. 126, no. 6, pp. 2123–2138, Jun. 2016, doi: 10.1172/JCI85309.
[24] W. C. Aird, "The role of the endothelium in severe sepsis and multiple organ dysfunction syndrome," *Blood*, vol. 101, no. 10, pp. 3765–3777, May 2003, doi: 10.1182/blood-2002-06-1887.
[25] Y. Wang *et al.*, "Coagulation Disorders after Chimeric Antigen Receptor T Cell Therapy: Analysis of 100 Patients with Relapsed and Refractory Hematologic Malignancies," *Biology of Blood and Marrow Transplantation*, Nov. 2019, doi: 10.1016/j.bbmt.2019.11.027.
[26] J. C. Chang, "Thrombocytopenia in critically ill patients due to vascular microthrombotic disease: pathogenesis based on 'two activation theory of the endothelium,'" *Vascul Dis Ther*, vol. 2, no. 5, 2017, doi: 10.15761/VDT.1000132.
[27] C. Probst, S. Schneider, and P. Loskill, "High-throughput organ-on-a-chip systems: Current status and remaining challenges," *Current Opinion in Biomedical Engineering*, vol. 6, pp. 33–41, Jun. 2018, doi: 10.1016/j.cobme.2018.02.004.
[28] C. A. Pennell *et al.*, "Human CD19-Targeted Mouse T Cells Induce B Cell Aplasia and Toxicity in Human CD19 Transgenic Mice," *Molecular Therapy*, vol. 26, no. 6, pp. 1423–1434, Jun. 2018, doi: 10.1016/j.ymthe.2018.04.006.
[29] M. Norelli *et al.*, "Monocyte-derived IL-1 and IL-6 are differentially required for cytokine-release syndrome and neurotoxicity due to CAR T cells," *Nature Medicine*, vol. 24, no. 6, Art. no. 6, Jun. 2018, doi: 10.1038/s41591-018-0036-4.
[30] A. Pfeiffer *et al.*, "In vivo generation of human CD19-CAR T cells results in B-cell depletion and signs of cytokine release syndrome," *EMBO Molecular Medicine*, vol. 10, no. 11, p. e9158, Nov. 2018, doi: 10.15252/emmm.201809158.
[31] T. Giavridis, S. J. C. van der Stegen, J. Eyquem, M. Hamieh, A. Piersigilli, and M. Sadelain, "CAR T cell–induced cytokine release syndrome is mediated by macrophages and abated by IL-1 blockade," *Nature Medicine*, vol. 24, no. 6, Art. no. 6, Jun. 2018, doi: 10.1038/s41591-018-0041-7.
[32] D. M. Reed *et al.*, "An autologous endothelial cell:peripheral blood mononuclear cell assay that detects cytokine storm responses to biologics," *The FASEB Journal*, vol. 29, no. 6, pp. 2595–2602, 2015, doi: 10.1096/fj.14-268144.
[33] X. Fu, A. Rivera, L. Tao, and X. Zhang, "Genetically modified T cells targeting neovasculature efficiently destroy tumor blood vessels, shrink established solid tumors and increase nanoparticle delivery," *International Journal of Cancer*, vol. 133, no. 10, pp. 2483–2492, 2013, doi: 10.1002/ijc.28269.

[34] S. Tettamanti *et al.*, "Targeting of acute myeloid leukaemia by cytokine-induced killer cells redirected with a novel CD123-specific chimeric antigen receptor," *British Journal of Haematology*, vol. 161, no. 3, pp. 389–401, 2013, doi: 10.1111/bjh.12282.
[35] V. Dhir *et al.*, "A predictive biomimetic model of cytokine release induced by TGN1412 and other therapeutic monoclonal antibodies," *Journal of Immunotoxicology*, vol. 9, no. 1, pp. 34–42, Mar. 2012, doi: 10.3109/1547691X.2011.613419.
[36] C. M. Metallo, M. A. Vodyanik, J. J. de Pablo, I. I. Slukvin, and S. P. Palecek, "The response of human embryonic stem cell-derived endothelial cells to shear stress," *Biotechnology and Bioengineering*, vol. 100, no. 4, pp. 830–837, 2008, doi: 10.1002/bit.21809.
[37] A. Deenadayalan, P. Maddineni, and A. Raja, "Comparison of whole blood and PBMC assays for T-cell functional analysis," *BMC Res Notes*, vol. 6, p. 120, Mar. 2013, doi: 10.1186/1756-0500-6-120.
[38] N. Singh *et al.*, "Monocyte lineage–derived IL-6 does not affect chimeric antigen receptor T-cell function," *Cytotherapy*, vol. 19, no. 7, pp. 867–880, Jul. 2017, doi: 10.1016/j.jcyt.2017.04.001.
[39] R. M. Sterner *et al.*, "GM-CSF inhibition reduces cytokine release syndrome and neuroinflammation but enhances CAR-T cell function in xenografts," *Blood*, vol. 133, no. 7, pp. 697–709, Feb. 2019, doi: 10.1182/blood-2018-10-881722.
[40] A. H. J. Tan, N. Vinanica, and D. Campana, "Chimeric antigen receptor–T cells with cytokine neutralizing capacity," *Blood Adv*, vol. 4, no. 7, pp. 1419–1431, Apr. 2020, doi: 10.1182/bloodadvances.2019001287.
[41] Y. Sun, S. Wang, L. Zhao, B. Zhang, and H. Chen, "IFN-gamma and TNF-alpha aggravate endothelial damage caused by CD123-targeted CAR T cell," *OncoTargets and Therapy*, Jun. 24, 2019. https://www.dovepress.com/ifn-gamma-and-tnf-alpha-aggravate-endothelial-damage-caused-by-cd123-t-peer-reviewed-article-OTT (accessed May 11, 2020).
[42] A. Shanti, J. Teo, and C. Stefanini, "In Vitro Immune Organs-on-Chip for Drug Development: A Review," *Pharmaceutics*, vol. 10, no. 4, Art. no. 4, Dec. 2018, doi: 10.3390/pharmaceutics10040278.
[43] J. A. Brown *et al.*, "Metabolic consequences of inflammatory disruption of the blood-brain barrier in an organ-on-chip model of the human neurovascular unit," *Journal of Neuroinflammation*, vol. 13, no. 1, p. 306, Dec. 2016, doi: 10.1186/s12974-016-0760-y.
[44] D. Nemcovsky Amar, M. Epshtein, and N. Korin, "Endothelial Cell Activation in an Embolic Ischemia-Reperfusion Injury Microfluidic Model," *Micromachines*, vol. 10, no. 12, Art. no. 12, Dec. 2019, doi: 10.3390/mi10120857.
[45] H. Uwamori, Y. Ono, T. Yamashita, K. Arai, and R. Sudo, "Comparison of organ-specific endothelial cells in terms of microvascular formation and endothelial barrier functions," *Microvascular Research*, vol. 122, pp. 60–70, Mar. 2019, doi: 10.1016/j.mvr.2018.11.007.
[46] A. Herland, A. D. van der Meer, E. A. FitzGerald, T.-E. Park, J. J. F. Sleeboom, and D. E. Ingber, "Distinct Contributions of Astrocytes and Pericytes to Neuroinflammation Identified in a 3D Human Blood-Brain Barrier on a Chip," *PLoS ONE*, vol. 11, no. 3, p. e0150360, Mar. 2016, doi: 10.1371/journal.pone.0150360.
[47] P. F. Costa *et al.*, "Mimicking arterial thrombosis in a 3D-printed microfluidic in vitro vascular model based on computed tomography angiography data," *Lab Chip*, vol. 17, no. 16, pp. 2785–2792, Aug. 2017, doi: 10.1039/C7LC00202E.
[48] D. B. Kolesky, R. L. Truby, A. S. Gladman, T. A. Busbee, K. A. Homan, and J. A. Lewis, "3D Bioprinting of Vascularized, Heterogeneous Cell-Laden Tissue Constructs," *Advanced Materials*, vol. 26, no. 19, pp. 3124–3130, 2014, doi: 10.1002/adma.201305506.
[49] X. Li and T. Tian, "Recent advances in an organ-on-a-chip: biomarker analysis and applications," *Anal. Methods*, vol. 10, no. 26, pp. 3122–3130, Jul. 2018, doi: 10.1039/C8AY00970H.
[50] R. G. Mannino *et al.*, "3D microvascular model recapitulates the diffuse large B-cell lymphoma tumor microenvironment in vitro," *Lab Chip*, vol. 17, no. 3, pp. 407–414, Jan. 2017, doi: 10.1039/C6LC01204C.

[51] Y. Zhu, F. Yin, H. Wang, L. Wang, J. Yuan, and J. Qin, “Placental Barrier-on-a-Chip: Modeling Placental Inflammatory Responses to Bacterial Infection,” *ACS Biomater. Sci. Eng.*, vol. 4, no. 9, pp. 3356–3363, Sep. 2018, doi: 10.1021/acsbiomaterials.8b00653.
[52] F. Sharifi *et al.*, “A Foreign Body Response-on-a-Chip Platform,” *Advanced Healthcare Materials*, vol. 8, no. 4, p. 1801425, 2019, doi: 10.1002/adhm.201801425.
[53] S. Biglari *et al.*, “Simulating Inflammation in a Wound Microenvironment Using a Dermal Wound-on-a-Chip Model,” *Advanced Healthcare Materials*, vol. 8, no. 1, p. 1801307, Jan. 2019, doi: 10.1002/adhm.201801307.
[54] V. V. Orlova, F. E. van den Hil, S. Petrus-Reurer, Y. Drabsch, P. ten Dijke, and C. L. Mummery, “Generation, expansion and functional analysis of endothelial cells and pericytes derived from human pluripotent stem cells,” *Nature Protocols*, vol. 9, no. 6, Art. no. 6, Jun. 2014, doi: 10.1038/nprot.2014.102.
[55] M. N. S. de Graaf *et al.*, “Scalable microphysiological system to model three-dimensional blood vessels,” *APL Bioengineering*, vol. 3, no. 2, p. 026105, Jun. 2019, doi: 10.1063/1.5090986.
[56] V. H. Huxley, F. E. Curry, and R. H. Adamson, “Quantitative fluorescence microscopy on single capillaries: alpha-lactalbumin transport,” *American Journal of Physiology-Heart and Circulatory Physiology*, vol. 252, no. 1, pp. H188–H197, Jan. 1987, doi: 10.1152/ajpheart.1987.252.1.H188.
[57] J. Schindelin *et al.*, “Fiji: an open-source platform for biological-image analysis,” *Nature Methods*, vol. 9, no. 7, Art. no. 7, Jul. 2012, doi: 10.1038/nmeth.2019.
[58] C. McQuin *et al.*, “CellProfiler 3.0: Next-generation image processing for biology,” *PLOS Biology*, vol. 16, no. 7, p. e2005970, Jul. 2018, doi: 10.1371/journal.pbio.2005970.
[59] K.-C. Kuo *et al.*, “Bioengineering vascularized tissue constructs using an injectable cell-laden enzymatically crosslinked collagen hydrogel derived from dermal extracellular matrix,” *Acta Biomaterialia*, vol. 27, pp. 151–166, Nov. 2015, doi: 10.1016/j.actbio.2015.09.002.
[60] I. Pereiro, A. F. Khartchenko, L. Petrini, and G. V. Kaigala, “Nip the bubble in the bud: a guide to avoid gas nucleation in microfluidics,” *Lab Chip*, vol. 19, no. 14, pp. 2296–2314, Jul. 2019, doi: 10.1039/C9LC00211A.
[61] L. L. Bischel, E. W. K. Young, B. R. Mader, and D. J. Beebe, “Tubeless microfluidic angiogenesis assay with three-dimensional endothelial-lined microvessels,” *Biomaterials*, vol. 34, no. 5, pp. 1471–1477, Feb. 2013, doi: 10.1016/j.biomaterials.2012.11.005.
[62] F. Garcia-Polite *et al.*, “Pulsatility and high shear stress deteriorate barrier phenotype in brain microvascular endothelium,” *J Cereb Blood Flow Metab*, vol. 37, no. 7, pp. 2614–2625, Jul. 2017, doi: 10.1177/0271678X16672482.
[63] W.-Y. Huang, T. J. Kemp, R. M. Pfeiffer, L. A. Pinto, A. Hildesheim, and M. P. Purdue, “Impact of Freeze-Thaw Cycles on Circulating Inflammation Marker Measurements,” *Cytokine*, vol. 95, pp. 113–117, Jul. 2017, doi: 10.1016/j.cyto.2017.02.016.
[64] Y. Qiu *et al.*, “Microvasculature-on-a-chip for the long-term study of endothelial barrier dysfunction and microvascular obstruction in disease,” *Nature Biomedical Engineering*, vol. 2, no. 6, Art. no. 6, Jun. 2018, doi: 10.1038/s41551-018-0224-z.
[65] R. W. D’Amico *et al.*, “Pulmonary Vascular Platform Models the Effects of Flow and Pressure on Endothelial Dysfunction in BMPR2 Associated Pulmonary Arterial Hypertension,” *Int J Mol Sci*, vol. 19, no. 9, Aug. 2018, doi: 10.3390/ijms19092561.
[66] Y. Zhang *et al.*, “ICAM-1 expression and organization in human endothelial cells is sensitive to gravity,” *Acta Astronautica*, vol. 67, no. 9, pp. 1073–1080, Nov. 2010, doi: 10.1016/j.actaastro.2010.06.027.
[67] Y. Huang, Q. Tan, R. Chen, B. Cao, and W. Li, “Sevoflurane prevents lipopolysaccharide-induced barrier dysfunction in human lung microvascular endothelial cells: Rho-mediated alterations of VE-cadherin,” *Biochemical and Biophysical Research Communications*, vol. 468, no. 1, pp. 119–124, Dec. 2015, doi: 10.1016/j.bbrc.2015.10.150.
[68] S. Klöß, S. Dehmel, A. Braun, M. J. Parnham, U. Köhl, and S. Schiffmann, “From Cancer to Immune-Mediated Diseases and Tolerance Induction: Lessons Learned From Immune Oncology

and Classical Anti-cancer Treatment," *Front. Immunol.*, vol. 11, 2020, doi: 10.3389/fimmu.2020.01423.

[69] A. A. for C. Research, "JCAR015 in ALL: A Root-Cause Investigation," *Cancer Discov*, vol. 8, no. 1, pp. 4–5, Jan. 2018, doi: 10.1158/2159-8290.CD-NB2017-169.

[70] T. Hünig, "The rise and fall of the CD28 superagonist TGN1412 and its return as TAB08: a personal account," *The FEBS Journal*, vol. 283, no. 18, pp. 3325–3334, 2016, doi: https://doi.org/10.1111/febs.13754.